Design and Synthesis of Self-Organizing Zwitterions and Their Functional Evaluation

Takuro Matsumoto

2016

Department of Biotechnology

Tokyo University of Agriculture and Technology

Table of Contents

Chapter 1

Introduction

Chapter 1

1-1 Ionic Liquids

1-1-1 Features of Ionic Liquids

Ionic liquids (ILs) are a class of organic salts that are in the liquid state at room temperature (Figure 1-1).[1] The earliest report of ILs was described by Paul Walden in 1914.[2] He found that ethylammonium nitrate melted at 12 °C, but it was not stable in the presence of moisture. Wilkes and Zaworotko performed the pioneering work on water-stable ILs in 1992.[3] They drastically accelerated the field of ILs by reporting that the imidazolium-based IL, 1-ethyl-3-methylimidazolium tetrafluoroborate, was stable in the presence of moisture. A number of ILs have been designed and synthesized, which are currently receiving significant attention as novel solvents in large research fields. These ILs have fascinating properties, which are quite different from those of conventional molecular solvents, such as negligible vapor pressure,[4] flame retardancy,[5] and high ionic conductivity.[6]

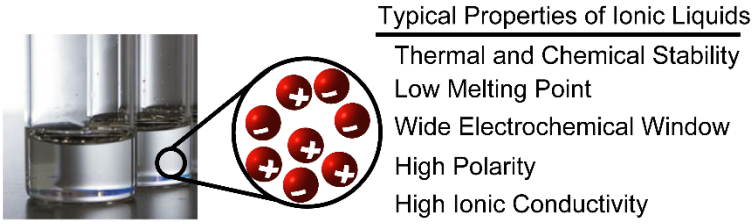

Figure 1-1. Photograph of ILs and their typical properties.

A key point of the construction of ILs with desirable properties is the design of the component ion structures. The representative ion species forming ILs are depicted in Figure 1-2. Quaternary onium cations, such as imidazolium, pyridinium, phosphonium, and ammonium ions, are widely used. These components have large structures and a delocalized charge. These factors weaken the electrostatic interaction between the cations and anions. As a result, they have a lower melting point. The chemical properties of ILs can be tuned by the selection of the cation and anion, which is the reason why ILs are often called designer solvents. For example, the melting points of ILs containing the 1-ethyl-3-methylimidazolium cation varied depending on the anion species: $[Cl]^-$ 89 °C > $[NO_3]^-$ 38 °C > $[BF_4]^-$ 15 °C > $[(CF_3SO_2)_2N]^-$ -15 °C.[7] ILs are a potential new generation of solvents due to their tunable chemical properties.

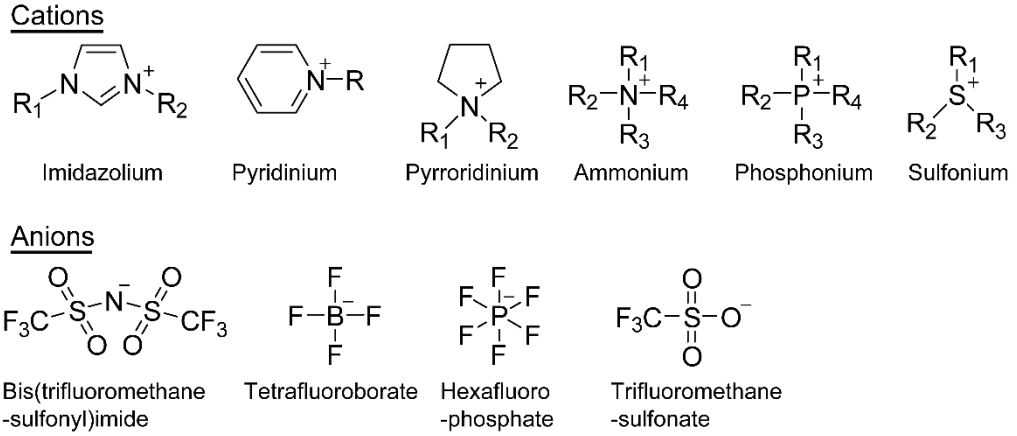

Figure 1-2. Representative ion species used for ILs.

1-1-2 Potential Applications of Ionic Liquids

For Solvents of Biopolymers

In recent years, inedible biomass has attracted significant attention as a new energy source. One of the major components of such biomass is cellulose, which is stabilized by multiple hydrogen bonds. Therefore, cellulose cannot dissolve into ordinary solvents, which hinders their use for bioenergy production. Rogers et al. first reported the dissolution of cellulose using ILs in 2002.[8] They prepared 1-butyl-3-methylimidazolium chloride, which dissolved cellulose above 100 °C (Figure 1-3). They also showed that the chloride anion penetrates the hydrogen bonding network between the hydroxy groups of cellulose due to their strong proton accepting ability. Recently, Ohno et al. determined that the use of both formate and phosphonate anions also endows ILs with a strong proton acceptor ability.[9] For example, 1-allyl-3-methylimidazolium formate dissolved cellulose at 60 °C due to its high polarity and low viscosity, but it was not thermally stable. Conversely, 1-ethyl-3-methylimidazolium dimethyl phosphate dissolved cellulose at room temperature and it had a high thermal stability. These results are one example that demonstrates that the suitable design of the ion structure endows ILs with desirable properties.

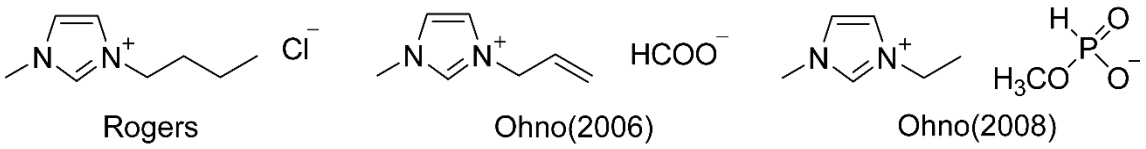

Figure 1-3. Representative ILs dissolving cellulose.

For Self-Assembly Media of Amphiphiles

In nature, water plays a key role as an essential solvent that affects the self-organization of amphiphiles. Amphiphiles form a variety of supramolecular structures, including micelles, vesicles, and liquid crystals. The self-organization behavior of amphiphiles in water is achieved by the hydrogen bonding ability of water, which enables the formation of interactions between the water molecules and amphiphiles. In recent years, a number of ILs (inspired by the water-based systems) have been reported that mediate self-organization behavior of amphiphiles.[10] In particular, there have been a strong interest in the use of protic ILs as self-assembly media of amphiphiles because they are capable of forming hydrogen bonds as readily as water. The representative ion species used for preparation of protic ILs are depicted in Figure 1-4.

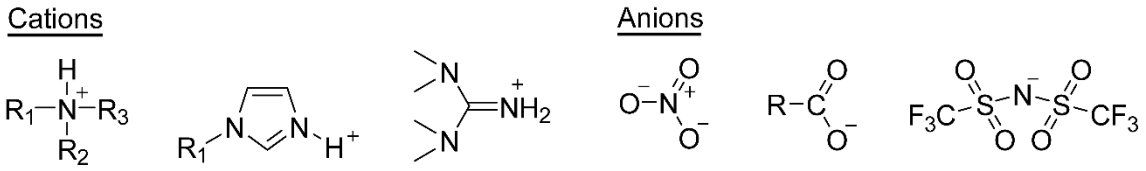

Figure 1-4. Representative ion species used for protic ILs.

Micelles are one of the representative self-organized structures of amphiphiles in water, which are formed though the segregation between polar and apolar parts of the amphiphiles. The apolar parts assemble and reject water, and the polar parts interact with water. In the 1980s, Evans and co-workers first demonstrated that alkyltrimethylammonium bromides and alkylpyridinium bromides formed micelles in the presence of ethylammonium nitrate.[11] While they share many similarities, hydrocarbons are more soluble in ethylammonium nitrate than in water. Therefore, the driving force for the exhibition of micelles is weakened. As a result, a higher critical micelle concentration was observed in the IL systems mentioned above. Following these reports, a large number of systematic studies comparing micelle formation in water and ILs have been performed. Micelle formation was also reported in a system consisting of an amphiphilic polymer and ILs. Lodge et al. have reported that a series of block copolymers form micelles in the presence of ILs.[12] For example, poly(styrene-*b*-methyl methacrylate) block copolymers formed micelles in the presence of 1-butyl-3-methylimidazolium hexafluorophosphate, which is a selective solvent for a poly(methyl methacrylate) segment. Thus, micelles formed by them have a polystyrene core and a poly(methyl methacrylate) shell.

Lyotropic liquid crystals are a class of self-organizing materials that form well-defined nanostructures in the presence of solvents. Since the first report of lyotropic liquid crystal formation in ILs was described in 1983 by Evans and co-workers using phospholipid and ethylammonium nitrate,[13] diverse liquid-crystalline (LC) phases, including micellar cubic, bicontinuous cubic,

columnar, and smectic phases, were observed in lyotropic LC systems with ILs.[14] While earlier reports mainly focused on protic ILs, the number of studies on lyotropic LC phases in the presence of aprotic ILs recently increased.[15] The formation of these aggregates is considered to be governed by the solvophobic and solvophilic interaction between amphiphiles and ILs. A number of ILs have a good affinity for the polar regions of amphiphiles but not with the apolar regions. These different solvation properties enhance the self-organization behavior of amphiphiles. More information on the collaboration of LC materials and ILs are described in section 1-2-1.

For Electrolytes of Batteries

In recent years, there have been attempts to apply ILs to electrochemical devices, including capacitors,[16] Li batteries,[17] fuel cells,[18] and solar cells.[19] These researches are motivated by fascinating characteristics of ILs, such as their high ionic conductivity, wide electrochemical potential window, flame retardant properties, and low vapor pressure. Although almost all ILs show high ionic conductivity, they do not contain electro active species for battery electrodes. Therefore, it is necessary to add target ions, such as lithium cations and protons, for practical use. For example, Watanabe et al. mixed 1-ethyl-3-methylimidazolium bis(trifluoromethylsulfonyl)imide and lithium bis(trifluoromethylsulfonyl)imide and evaluated their ionic conductivity. The ionic conductivity of the IL slightly decreased with the addition of lithium salt, which was attributed to an increase in the viscosity.[20] Protic ILs were widely used in fuel cells. They can be easily prepared by mixing Brønsted acids and bases.[21] To date, diverse strategies have been proposed to improve their electrolyte properties. The combination of ILs and polymers is also considered a potential approach to overcome the drawbacks of ILs.[22] Zwitterionization of ILs would be an effective approach to develop ILs as electrolytes. Details on zwitterions are described in section 1-3.

1-2 Organization of Ionic Liquids into Ordered States

Generally, ILs show isotropic properties because they form a liquid state at a large range of temperatures. If ILs are aligned into ordered states, they can be expected to show structure dependent properties derived from their ordered morphologies. In this section, the author introduces researches related to the ordered ILs using the self-organization behavior of LC compounds and block copolymers.

1-2-1 Liquid-Crystalline Ionic Liquids

Classification of Liquid Crystals

Liquid crystals are a class of soft materials that show properties of both crystals and liquids.[23] In general, LC phases are divided into two classes: lyotropic LC phases and thermotropic LC phases.

Lyotropic LC phases are induced in the presence of solvents, while thermotropic LC phases are determined or changed by temperature.

One of the most famous LC phases is a nematic LC phase. Nematic phases possess comparatively high fluidity because they have molecular direction without any long range periodicity. In addition, their molecular direction can be easily controlled by external stimuli. Thus, they have been used for optical displays. The typical LC molecules forming nematic LC phases are depicted in Figure 1-5. They have both a rigid and flexible part. Aromatic rings and long alkyl chains are frequently used for the rigid and flexible parts, respectively. When nanosegregation is induced in these LC molecules, they exhibit various nanosegregated LC phases.

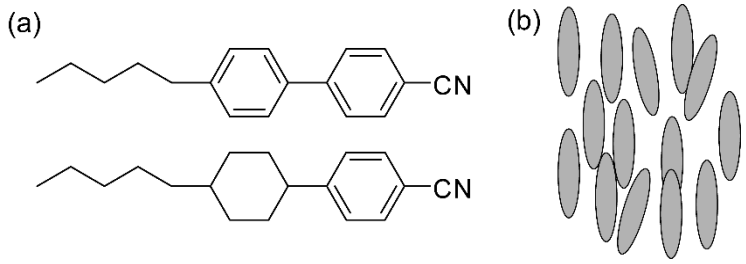

Figure 1-5. (a) Representative molecules forming nematic LC phases. (b) Schematic illustration of nematic LC phases.

In contrast to nematic LC phases, nanosegregated LC phases possess both molecular direction and long-range periodicity. They are formed by block molecules with two incompatible parts (e.g., hydrophilic/hydrophobic, ionophobic/ionophilic). Nanosegregation is induced between the incompatible parts at a molecular scale, which leads to a variety of nanostructured phases. The mesophase pattern of the nanosegregated LC phases mainly depends on the volume fraction of the incompatible parts. Tschierske et al. systematically studied the relationships between the morphology of the LC phases and the molecular structure.[24] They synthesized a series of amphiphilic molecules with hydrophilic polyhydroxy groups and hydrophobic long alkyl chains and investigated their LC phase behavior (Figure 1-6). For example, compound **3** self-organized into a smectic phase through nanosegregation between the incompatible parts, while compound **1-2,** having multiple long alkyl chains, exhibited inverted-type bicontinuous cubic and columnar phases which consisted of hydrophilic channels and hydrophobic sheath domains. In contrast, compound **4-5** showed the normal LC phases, with hydrophobic channel and hydrophilic sheath domains.

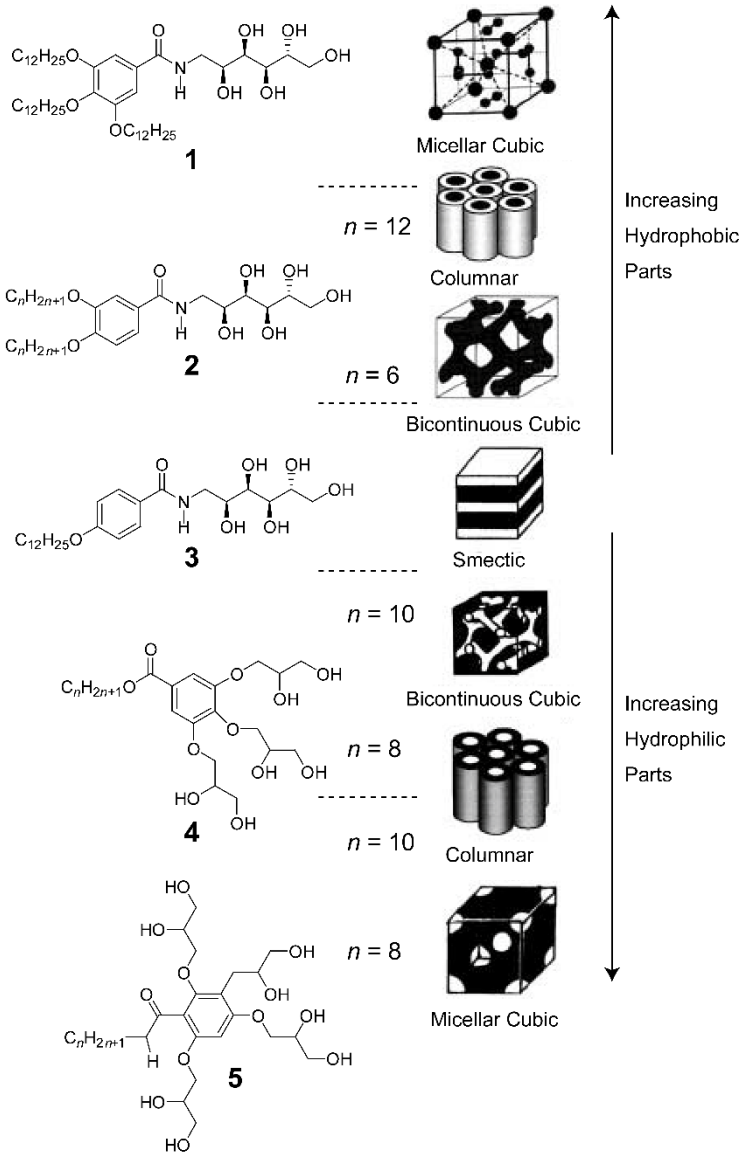

Figure 1-6. Dependence of the mesophase patterns on the molecular structure of amphiphiles.

Liquid-Crystalline Ionic Liquids

There are two strategies for the introduction of LC properties into ILs. One is mixing ILs with amphiphiles, which induces lyotropic LC phases. In this system, ILs are co-organized into ionophilic domains of LC structures with ionophilic amphiphiles, as described in section 1-1-2. The other is the introduction of thermotropic LC properties into ILs through the attachment of a nonionic part to the ILs.[25]

Ionic liquid crystals are a class of LC materials that consist of a cation and anion.[26] They are considered to show both properties of LC materials and ILs. Thus, their properties can be controlled through the selection of the cation and anion. The design of ionic LC molecules is based on the connection between ionic and nonionic parts. Typical ionic LC molecules are shown in Figure 1-7. A variety of ion species, such as quaternary phosphonium,[27] imidazolium,[28] and pyridinium,[29] are widely used. The self-organization behavior is strongly governed by the volume balance between the incompatible regions, as for nonionic LC compounds. Another point for controlling their phase behavior is the selection of ion species.[30] For example, the order of the mesophase stability of 1-alkyl-3-methylimidazolium salts varied depending on their anion species: $[Cl]^- > [Br]^- > [BF_4]^- > [CF_3SO_3]^- > [(CF_3SO_2)_2N]^-$.[31] The anion species of ionic liquid crystals affect not only their thermal behavior, but also their mesophase patterns. For example, Kim et al. have reported LC phase behavior of a series of guanidinium salts.[32] The guanidinium salts with NO_3 and BF_4 anions formed only columnar phases, while that with Cl anion formed both the columnar and micellar cubic phase.

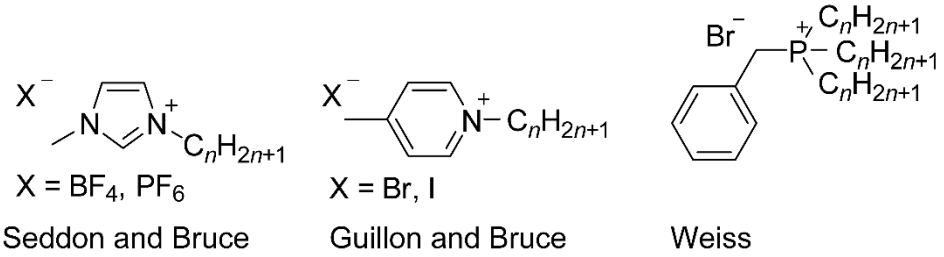

Figure 1-7. Representative molecules forming nanosegregated LC phases.

The mesophase patterns of nanosegregated LC materials are strongly governed by their molecular shape. Kato and Ohno's group studied the relationship between molecular shapes of ionic LC compounds and their mesophase patterns. They also determined that the introduction of LC properties to ILs induced morphology-dependent properties through the investigation of their ion conduction behavior.[33]

Ohno et al. have studied mesophase behavior of rod-shaped imidazolium salts,[34] such as 1-ethyl-3-dodecylimidazolium dodecylsulfonate (Figure 1-8).[35] It self-organized into a smectic phase in the presence or absence of lithium salts. Ion conduction measurements were performed, focusing on the ion conductive direction, i.e., parallel or perpendicular to the ionic layer. The series of salts showed anisotropic ion conduction properties in the LC state. The ionic conductivities varied depending on their morphology: the ionic conductivity parallel to the ionic layer was higher than that perpendicular to the ionic layer. This is because the long alkyl chain layer plays a role as insulating domains, while the IL layer plays a role as ion transport domains for ion conduction.

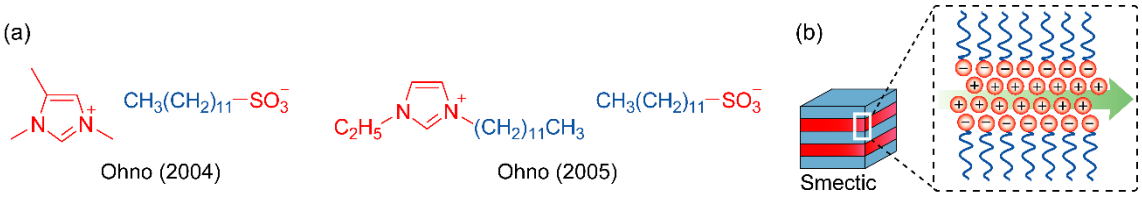

Figure 1-8. (a) Rod-shaped imidazolium salts forming smectic phases. (b) Schematic illustration of anisotropic ion conduction behavior observed for an ionic smectic phase.

Kato et al. prepared wedge-shaped imidazolium salts.[36] They introduced multiple long alkyl chains into imidazolium salts that formed columnar phases with ion channel and nonionic sheath domains. The columns were successfully aligned perpendicular and parallel to the elctrodes.[37] They also showed an anisotropic conductive behavior. In 2007, Kato et al. also reported phase behavior of wedge-shaped ammonium salts (Figure 1-9). These molecules exhibited columnar and bicontinuous cubic phases, which were dependent on the alkyl chain length. In particular, the obtained bicontinuous cubic LC materials showed unique ion conductive behavior. While the ionic conductivity in the bicontinuous cubic phase increased with elevating temperature, it suddenly decreased at the phase transition from the bicontinuous cubic phase to isotropic phase. Note the ionic conductivity measurement was performed for LC molecules without any alignment methods. These results suggest that nanochannels of bicontinuous cubic phases were interconnected and functioned as a 3D continuous ion conductive pathway.

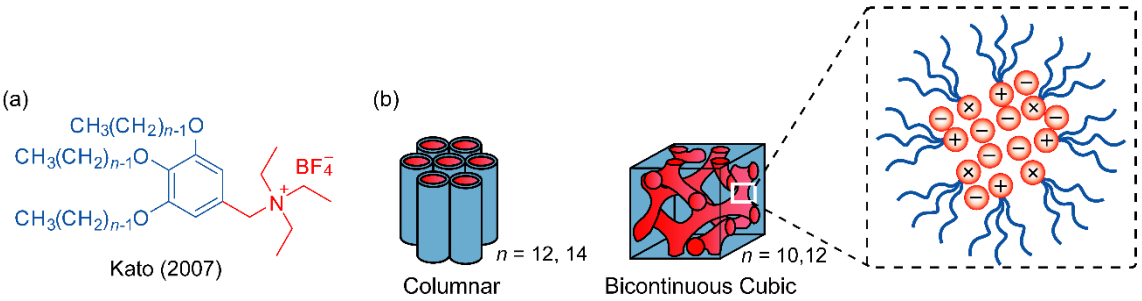

Figure 1-9. (a) Representative wedge-shaped ammonium salts. (b) Schematic illustration of the columnar and bicontinuous cubic phase transporting ions along the nanochannels.

1-2-2 Polymerized Ionic Liquid Block Copolymers

Polymerized Ionic Liquids

Polymerized ionic liquids (PILs) were reported for the first time by Ohno et al. in 1998.[38] They reported a glass transition temperature, T_g = -75.4 °C for a polymerized *N*-vinyl-3-ethylimidazolium bis(trifluoromethanesulfonyl)imide, and T_g = -76.5 °C for the monomer. The low T_g values of PILs (an intrinsic property in spite of their high charge density) eventually caught the attention of polymer scientists. To apply PILs to polyelectrolytes for batteries and fuel cells, numerous efforts have been devoted to lowering their T_g.[39] In this context, a number of PIL based materials have been reported, including polycation or polyanion-type PILs, PIL random copolymers, PIL block copolymers, and polymerized zwitterions (Figure 1-10). In particular, PIL block copolymers have attracted significant attention from electrolyte fields.[40]

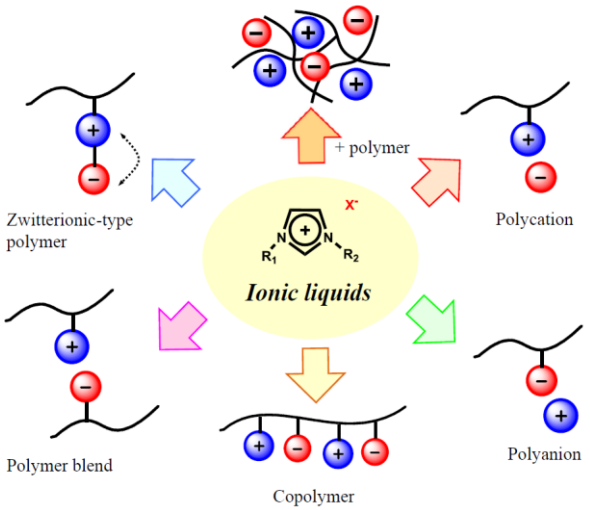

Figure 1-10. Schematic illustration of a series of PILs.

Polymerized Ionic Liquid Block Copolymers

In general, block copolymers with incompatible blocks form microphase-separated structures due to their segregation. Their morphologies are similar to that of the nanosegregated LC materials, but block copolymers form a well-ordered state at a macroscopic scale. The exhibition of microphase-separated structures is related to various factors, such as molecular weight, volume fraction, and component species. Masten et al. mapped out the morphology diagram of neutral-neutral diblock copolymers by self-consistent field theory.[41] The diagram in Figure 1-11 is described as a function of χN and f. The Flory-Huggins interaction parameter of the two blocks, the overall degree of polymerization, and volume fraction of the blocks are indicated by χ, N, and f, respectively. These predictions show a good

agreement with the experimental studies.[42] However, studies of the self-assembly of neutral-charged diblock copolymers are limited. Several researchers have pointed out that the observations for neutral-neutral diblock copolymers systems cannot be applied to neutral-charged diblock copolymer systems.[40, 43] The use of charged functional groups as building blocks of block copolymers makes it more difficult to predict their phase behavior.[44] In particular, Coulomb interactions among the charged groups complicate the understanding of their self-organization behavior by using theoretical calculations and simulation studies.

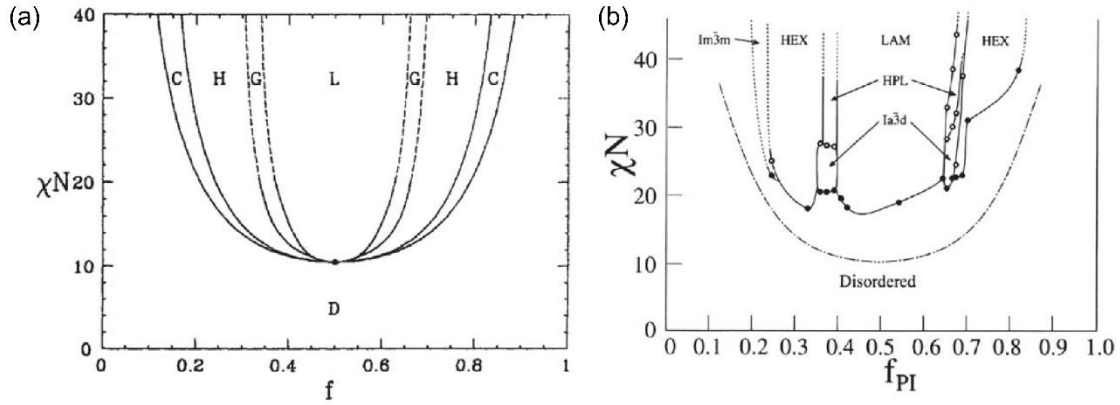

Figure 1-11. (a) A phase diagram of microphase-separated structures of diblock copolymers. L/LAM, lamellae; G/*Ia3d*, gyroid; H, hexagonally packed cylinder; C/*Im3m*, sphere; D, disordered. (b) Experimental results on diblock copolymers composed of polystyrene and polyisoprene.

In the last decades, PILs became attractive as one component of block copolymers due to their unique properties, such as their low T_g in spite of their high charge density.[45] The morphology of the microphase-separated structures formed by the PIL block copolymers are strongly governed by component species of block copolymers. Winey et al. synthesized poly(methylmethacrylate-*b*-1-[2-methacryloyloxy]ethyl)-3-butylimidazolium bis(trifluoromethanesulfonyl)imide via reversible addition-fragmentation chain transfer polymerization (Figure 1-12).[46] Their bulk-state morphologies were investigated using small-angle X-ray scattering (SAXS) measurements and transmission electron microscopy (TEM) and they did not exhibit microphase-separated structures with long-range periodicity. Alternatively, poly(styrene-*b*-1-[2-methacryloyloxy]ethyl)-3-butylimidazolium bis(trifluoromethanesulfonyl)imide (S-*b*-MEBIm-TFSI) formed microphase-separated structures with long-range periodicity. For example, the SAXS profile of S-*b*-MEBIm-TFSI containing 17.0 mol% PIL exhibited scattering peaks at q*, 2q*, and 3q* positions, which indicates a lamellae structure. Their morphology differences are explained by the miscibility of each block. While poly(methylmethacrylate) blocks were partially miscible with the PIL blocks, polystyrene blocks were

not compatible with the PIL blocks. Thus, the suitable selection of component species for PIL block copolymers is important to control their microphase-separated structures.

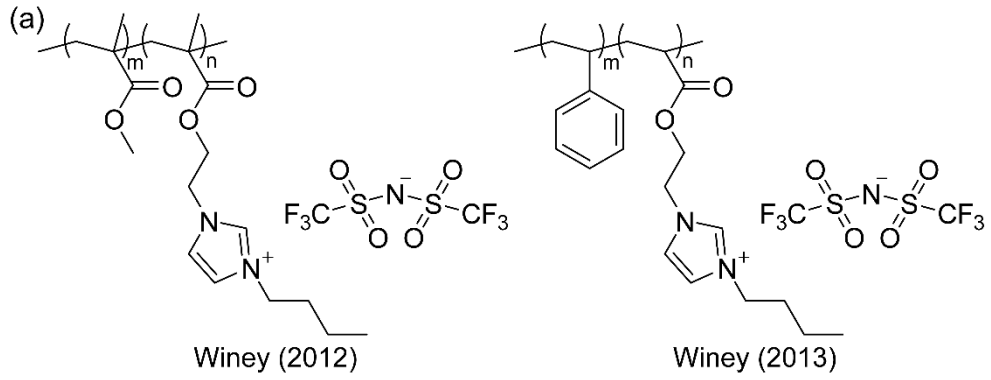

Figure 1-12. Chemical structures of (a) poly(methyl methacrylate-*b*-imidazolium salt) diblock copolymer and (b) poly(styrene-*b*-imidazolium salt) diblock copolymer.

Gin et al. also reported microphase-separated structures of PIL diblock copolymers.[47] They synthesized alkyl substituted norbornene-imidazolium salt diblock copolymers using living ring-opening metathesis polymerization and studied their morphology (Figure 1-13). Various microphase separated-structures were observed, reflecting a component ratio of two blocks. For example, the diblock copolymers containing 42–62 vol% of norbornene dodecyl ester exhibited lamellae structures, while hexagonally packed cylinders were observed for the diblock copolymers containing 64–81 vol% of norbornene dodecyl ester in a solvent-free melt state.

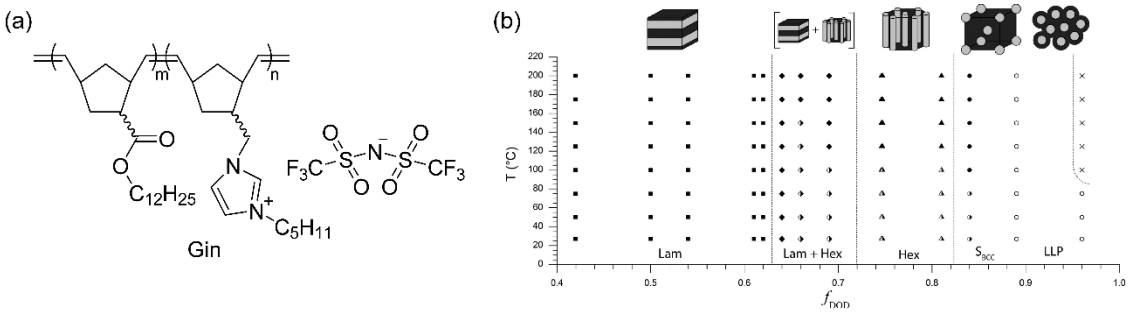

Figure 1-13. (a) Chemical structure of alkyl substituted norbornene–imidazolium salt diblock copolymers. (b) A phase diagram of morphology observed for the diblock copolymers.

Block copolymerization of PIL would be one of the promising approaches for the development of ion conductive materials that fulfill both high ionic conductivity and mechanical stability. In 2012,

Mahantthapa et al. investigated the relationship between the morphology of the microphase-separated structures and their ion conduction behavior (Figure 1-14).[48] They synthesized polystyrene-*b*-4-vinylbenzyl-alkylimidazolium bis(trifluoromethanesulfonyl)imide via nitroxide-mediated polymerization. They formed well-ordered microphase-separated structures that showed higher ionic conductivities than samples with less order. For example, the structure containing 8.6 mol% PIL in a well-ordered state showed around one order magnitude higher ionic conductivities than samples without long-range order. These results suggest that the use of PIL block copolymers is useful for the construction of ion conductive materials.

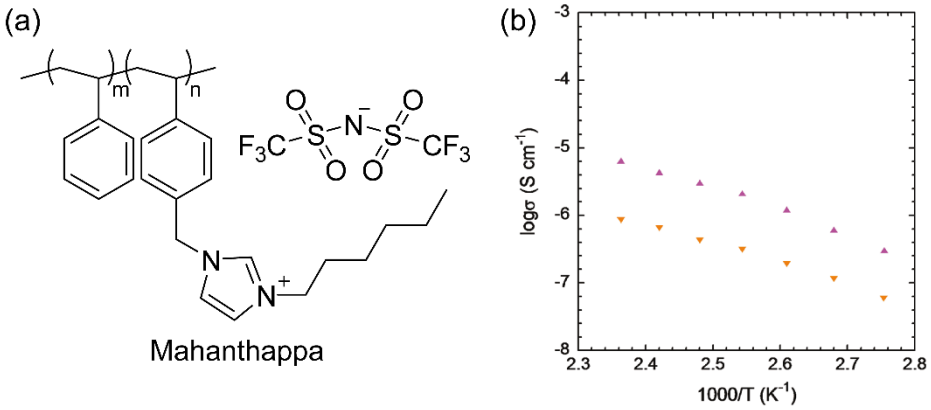

Figure 1-14. (a) Chemical structure of polystyrene-*b*-4-vinylbenzyl-alkylimidazolium bis(trifluoromethanesulfonyl)imide. (b) Ionic conductivity of the polymer films with long range order (▲) and without one (▼).

1-3 Zwitterions as Derivatives of Ionic Liquids

Many studies of ILs have been motivated by their intrinsic high ionic conductivity. However, the transported ion components in IL-based systems are useless for the electrolyte solutions of batteries and fuel cells. It is necessary to transport lithium ions and protons selectively to develop lithium ion batteries and fuel cells, respectively. Although ILs have some advantageous characteristics for electrolytes, such as a negligible vapor pressure, flame retardant properties, and the dissociation ability for added salts or acids, their migration inhibits selective transportation of target ions. In 2001, Ohno et al. reported the design of ILs to disturb the migration of ILs.[49] They synthesized a series of zwitterions in which cations and anions were covalently tethered. Since zwitterions are intermolecularly neutral, they did not migrate under a potential gradient (Figure 1-15).

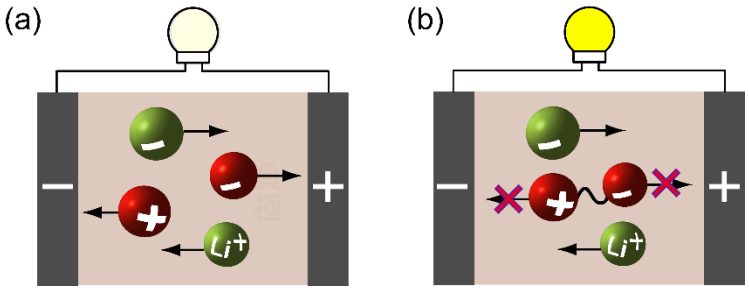

Figure 1-15. Schematic illustration of (a) ILs and (b) zwitterions under a potential gradient

Typical ion components of zwitterions are shown in Figure 1-16.[50] Generally, they have a higher melting point than ILs because their cation and anion are tethered. It is noteworthy that their thermal behavior was drastically changed upon the addition of lithium salts. For example, pristine imidazolium-based zwitterions, such as 1-ethyl-3-sulfopropyl imidazolium betaine, is solid at room temperature, but it becomes a homogeneous liquid in the presence of an equimolar amount of lithium bis(trifluoromethanesulfonyl)imide (Figure 1-17). This phase change is attributed to an ion exchange between the zwitterions. It was previously shown that the cation of zwitterions and the anion of added salts form IL-like ion pairs preferentially due to the hard and soft, acids and bases principle. Furthermore it has been already revealed that they selectively transport additive cations.

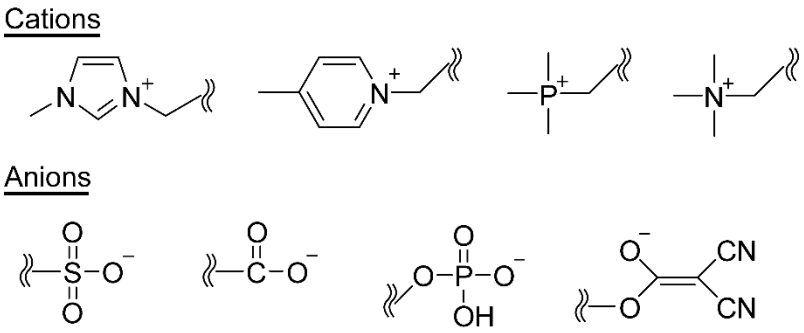

Figure 1-16. Representative ion species used for zwitterions.

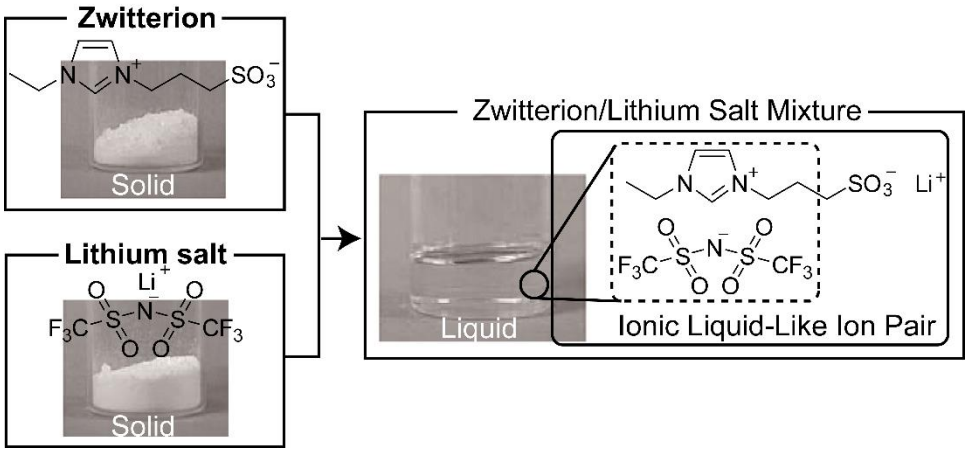

Figure 1-17. Chemical structure of imidazolium-based zwitterion and added lithium salt, and their photograph.

The use of zwitterions in electrochemical devices started to attract significant attention after studies on their physicochemical properties.[51] MacFarlane et al. reported on the on electrochemical effects of adding zwitterions to polyelectrolytes.[52] For example, they prepared polyelectrolyte gels using a random copolymer of 10 wt% lithium 2-acrylamido-2-methyl-1-propanesulphonic acid and 90 wt% *N*, *N*′-dimethylacryl amide with propylene carbonate as a solvent. The ion conductivities of the gel increased upon the addition of the zwitterion (Figure 1-18). The addition of the zwitterion also enhanced the ionic conductivity of the TiO_2 filler gels at an optimum filler concentration, while further addition of filler above the optimum concentration caused a decrease in conductivity. An increase of the lithium ion mobility upon the addition of zwitterions was also confirmed using ^{7}Li NMR measurements.

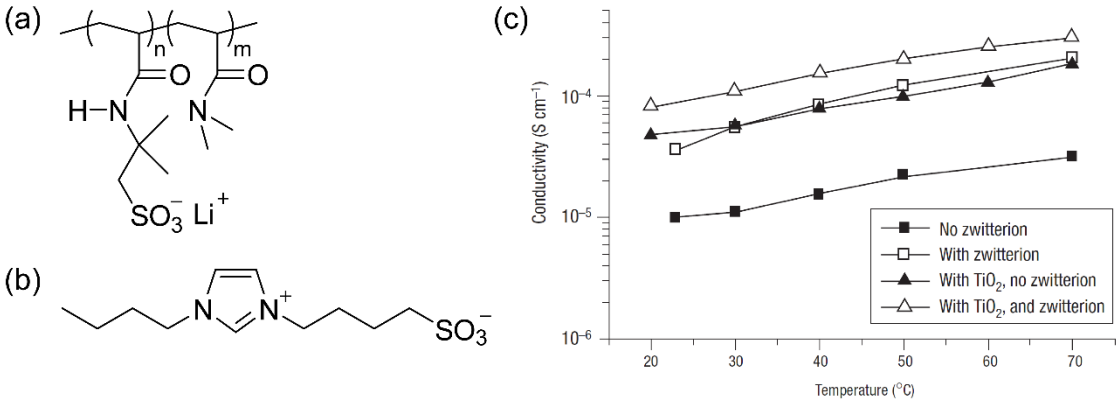

Figure 1-18. A combination of (a) polyelectrolyte and (b) zwitterions for inducing the gels in the presence of propylene carbonate. Their ionic conductivities were depicted in (c).

Long et al. determined that zwitterions are swollen with high polar ILs and they fabricated electromechanical transducers (Figure 1-19).[53] In the case of the sulfobetaine methacrylamide-*co*-butyl acrylate copolymers, an increase of the IL uptake was observed with the increase of zwitterion content. These results showed that zwitterions had a large affinity for polar ILs. The introduction of a polymerized zwitterion into the ABA triblock copolymers also enhanced the affinity for ILs, which induced rubbery plateau moduli of around 100 MPa and electromechanical actuation to electrical stimuli.

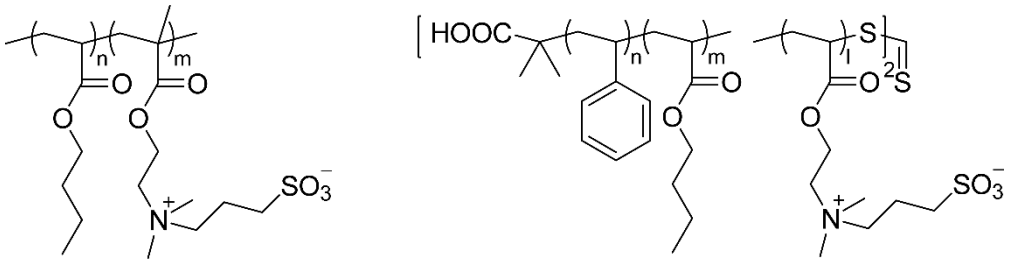

Long (2011) Long (2012)

Figure 1-19. Representative polymerized zwitterion copolymers.

1-4 Objectives and Thesis Outline

Parallel to the progress in IL studies as functional liquid materials, there has been growing attention to the development of the derivatives of ILs to accelerate their functionalization in diverse research fields. A representative example is zwitterions in which cations and anions are covalently tethered. Our research has been motivated by the following reasons: (1) Zwitterions have an ability to form a homogeneous complex with some lithium salts or acids, providing a liquid medium with a low T_g, which is reminiscent of ILs. (2) The obtained liquid medium functions as an ion active matrix that selectively transports the lithium cations or protons because zwitterions themselves never respond to a potential gradient due to their ion structures having zero net charge. While these studies have proceeded by focusing on the unique features of the mixture of zwitterions and acids or salts as liquid materials, the author expected that the introduction of self-organizing properties into zwitterions would lead to the expansion of the function design of zwitterions. In particular, the author focused on phase separated structures, such as nanosegregated assemblies formed by LC materials and microphase-separated assemblies formed by block copolymers, as one of the effective ways to accelerate the functionalization of zwitterions because it has been gradually revealed that the use of these self-organizing materials allocates incompatible properties onto their different domains. In this context, the

author envisioned that it would be possible to endow zwitterions with new properties without the loss of their intrinsic functions by introducing self-organizing properties to zwitterions.

The objective of this thesis is to accumulate basic insight on the design of self-organizing zwitterions.

Chapter 1 introduces ILs and describes their derivatives. This chapter also describes the objective of this thesis.

In chapter 2, the synthesis of a series of pyridinium-based amphiphilic zwitterions are described. The effect of the addition of additives on their nanosegregated structures and ion conductive properties are discussed through the investigation of their phase behavior in the presence/absence of acids or lithium salts.

Chapter 3 discusses the LC properties of gemini imidazolium-based amphiphilic zwitterions. The results led us to conclude that the use of the LC systems composed of amphiphilic zwitterions and acids or salts is useful to control the thermotropic LC phase behavior of a series of amphiphilic zwitterions. Furthermore, the author clearly observed ion conduction behavior that was dependent on the assembled states.

In chapter 4, the author employed polyzwitterions as building blocks of block copolymers. Poly(styrene-*b*-ammonium-based zwitterion) block copolymers formed microphase-separated structures composed of aggregated micelles containing a polystyrene core and polyzwitterion shell. Incorporation of lithium salts into the assemblies, setting up IL-like ion pairs, endowed a three dimensionally connected polyzwitterion domain with ion transporting ability.

Chapter 5 presents the conclusions of this thesis.

1-5 References

1. M. Armand, F. Endres, D. R. MacFarlane, H. Ohno, B. Scrosati, *Nat. Mater*., **2009**, *8*, 621.
2. P. Walden, *Bull. Acad. Sci*. (St Petersburg), **1914**, 405.
3. J. S. Wilkes, M. J. Zaworotko, *J. Chem. Soc., Chem. Commun*., **1992**, 965.
4. M. J. Earle, J. M. S. S. Esperança, M. A. Gilea, J. N. C. Lopes, L. P. N. Rebelo, J. W. Magee, K. R. Seddon, J. A. Widegren, *Nature*, **2006**, *439*, 831.
5. M. Smiglak, W. M. Reichert, J. D. Holbrey, J. S. Wilkes, L. Sun, J. S. Thrasher, K. Kirichenko, S. Singh, A. R. Katritzky, R. D. Rogers, *Chem. Commun*., **2006**, 2554.
6. P. Bonhôte, A.-P. Dias, N. Papageorgiou, K. Kalyanasundaram, M. Grätzel, *Inorg. Chem*., **1996**, *35*, 1168.
7. S. Zhang, N. Sun, X. He, X. Lu, X. Zhang, *J. Phys. Chem. Ref. Data*, **2006**, *35*, 1475.
8. R. P. Swatloski, S. K. Spear, J. D. Holbrey, R. D. Rogers, *J. Am. Chem. Soc*., **2002**, *124*, 4974.
9. (a) Y. Fukaya, A. Sugimoto, H. Ohno, *Biomacromolecules*, **2006**, *7*, 3295. (b) Y. Fukaya, K.

Hayashi, M. Wada, H. Ohno, *Green Chem*., **2008**, *10*, 44.

10. T. L. Greaves, C. J. Drummond, *Chem. Rev*., **2008**, *108*, 206.
11. (a) D. F. Evans, A. Yamauchi, R. Roman, E. Z. Casassa, *J. Colloid Interface Sci.*, **1982**, *88*, 89. (b) D. F. Evans, A. Yamauchi, G. J. Wei, V. A. Bloomfield, *J. Phys.Chem.*, **1983**, *87*, 3537.
12. (a) Y. He, Z. Li, P. Simone, T. P. Lodge, *J. Am. Chem. Soc*., **2006**, *128*, 2745. (b) P. M. Simone, T. P. Lodge, *Macromol. Chem. Phys*., **2007**, *208*, 339. (c) P. M. Simone, T. P. Lodge, *Macromolecules*, **2008**, *41*, 1753.
13. D. F. Evans, E. W. Kaler, W. J. Benton, *J. Phys. Chem*., **1983**, *87*, 533.
14. (a) T. L. Greaves, C. J. Drummond, *Chem. Soc. Rev.*, **2008**, *37*, 1709. (b) X. Mulet, D. F. Kennedy, T. L. Greaves, L. J. Waddington, A. Hawley, N. Kirby, C. J. Drummond, *J. Phys. Chem. Lett.*, **2010**, *1*, 2651.
15. (a) N. Kimizuka, T. Nakashima, *Langmuir*, **2001**, *17*, 6759. (b) T. Ichikawa, M. Yoshio, S. Taguchi, J. Kagimoto, H. Ohno, T. Kato, *Chem. Sci.*, **2012**, *3*, 2001.
16. M. Galiński, A. Lewandowski, I. Stępniak, *Electrochim Acta*, **2006**, *51*, 5567.
17. B. Scrosati, J. Garche, *J. Power Sources*, **2010**, *195*, 2419.
18. D. R. MacFarlane, M. Forsyth, P. C. Howlett, J. M. Pringle, J. Sun, G. Annat, W. Neil, E. I. Izgorodina, *Acc. Chem. Res.*, **2007**, *40*, 1165.
19. A. Hagfeldt, G. Boschloo, L. Sun, L. Kloo, H. Pettersson, *Chem. Rev*., **2010**, *110*, 6595.
20. S. Seki, Y. Kobayashi, H. Miyashiro, Y. Ohno, A. Usami, Y. Mita, N. Kihira, M. Watanabe, N. Terada, *J. Phys. Chem. B*, **2006**, *110*, 10228.
21. A. Noda, M. A. B. H. Susan, K. Kudo, S. Mitsushima, K. Hayamizu, M. Watanabe, *J. Phys. Chem. B*, **2003**, *107*, 4024.
22. T. Ueki, M. Watanabe, *Macromolecules*, **2008**, *41*, 3739.
23. (a) Handbook of Liquid Crystals (Eds.: D. Demus, J. W. Goodby, G.W. Gray, H.-W. Spiess, V. Vill), Wiley-VCH, Weinheim, **1998**. (b) T. Kato, *Science*, **2002**, *295*, 2414.
24. P. Fuchs, C. Tschierske, K. Raith, K. Das, S. Diele, *Angew. Chem. Int. Ed*., **2002**, *41*, 628.
25. T. Kato, N. Mizoshita, K. Kishimoto, *Angew. Chem. Int. Ed*., **2006**, *45*, 38.
26. J. D. Holbrey, K. R. Seddon, *J. Chem. Soc., Dalton Trans*., **1999**, 2133.
27. D. J. Abdallah, A. Robertson, H.-F. Hsu, R. G. Weiss, *J. Am. Chem. Soc*., **2000**, *122*, 3053.
28. C. J. Bowlas, D. W. Bruce, K. R. Seddon, *Chem. Commun*., **1996**, 1625.
29. D. W. Bruce, S. Estdale, D. Guillon, B. Heinrich, *Liq. Cryst*., **1995**, *19*, 301.
30. (a) K. Binnemans, *Chem. Rev*., **2005**, *105*, 4148. (b) M. Yoshio, T. Ichikawa, H. Shimura, T. Kagata, A. Hamasaki, T. Mukai, H. Ohno, T. Kato, *Bull. Chem. Soc. Jpn*., **2007**, *80*, 1836.
31. A. E. Bradley, C. Hardacre, J. D. Holbrey, S. Johnston, S. E. J. McMath, M. Nieuwenhuyzen, *Chem. Mater.*, **2002**, *14*, 629.
32. D. Kim, S. Jon, H.-K. Lee, K. Baek, N.-K. Oh, W.-C. Zin, K. Kim, *Chem. Commun*., **2005**, 5509.

33. M. Funahashi, H. Shimura, M. Yoshio, T. Kato, *Struct. Bond*., **2008**, *128*, 151.
34. (a) T. Mukai, M. Yoshio, T. Kato, H. Ohno, *Chem. Lett.*, **2004**, *33*, 1630. (b) T. Mukai, M. Yoshio, T. Kato, M. Yoshizawa-Fujita, H. Ohno, *Electrochemistry*, **2005**, *73*, 623. (c) T. Mukai, M. Yoshio, T. Kato, H. Ohno, *Chem. Lett*., **2005**, *34*, 442.
35. T. Mukai, M. Yoshio, T. Kato, M. Yoshizawa, H. Ohno, *Chem. Commun*., **2005**, 1333.
36. (a) T. Ichikawa, M. Yoshio, A. Hamasaki, T. Mukai, H. Ohno, T. Kato, *J. Am. Chem. Soc.*, **2007**, *129*, 10662. (b) H. Shimura, M. Yoshio, K. Hoshino, T. Mukai, H. Ohno, T. Kato, *J. Am. Chem. Soc*., **2008**, *130*, 1759. (c) A. E. Frise, S. V. Dvinskikh, H. Ohno, T. Kato, I. Furó, *J. Phys. Chem. B*, **2010**, *114*, 15477. (d) A. E. Frise, T. Ichikawa, M. Yoshio, H. Ohno, S.V. Dvinskikh, T. Kato, I. Furó, *Chem. Commun.*, **2010**, *46*, 728.
37. M. Yoshio, T. Mukai, H. Ohno, T. Kato, *J. Am. Chem. Soc*., **2004**, *126*, 994.
38. H. Ohno, K. Ito, *Chem. Lett*., **1998**, *27*, 751.
39. (a) E. B. Anderson, T. E. Long, *Polymer*, **2010**, *51*, 2447. (b) J. Yuan, M. Antonietti, *Polymer*, **2011**, *52*, 1469. (c) D. Mecerreyes, *Prog. Polym. Sci*., **2011**, *36*, 1629. (d) J. Yuan, D. Mecerreyes, M. Antonietti, *Prog. Polym. Sci.*, **2013**, *38*, 1009. (e) N. Nishimura, H. Ohno, *Polymer*, **2014**, *55*, 3289.
40. X. Wang, M. Goswami, R. Kumar, B. G. Sumpter, J. Mays, *Soft Matter*, **2012**, *8*, 3036.
41. M. W. Matsen, M. Schick, *Phys. Rev. Lett.*, **1994**, *72*, 2660.
42. A. K. Khandpur, S. Forster, F. S. Bates, I. W. Hamley, A. J. Ryan, W. Bras, K. Almdal, K. Mortensen, *Macromolecules*, **1995**, *28*, 8796.
43. M. J. Park, N. P. Balsara, *Macromolecules*, **2008**, *41*, 3678.
44. (a) M. Goswami, S. K. Kumar, A. Bhattacharya, J. F. Douglas, *Macromolecules*, **2007**, *40*, 4113. (b) M. Goswami, R. Kumar, B. G. Sumpter, J. Mays, *J. Phys. Chem. B*, **2011**, *115*, 3330.
45. Y. Gu, T. P. Lodge, *Macromolecules*, **2011**, *44*, 1732.
46. (a) J.-H. Choi, Y. Ye, Y. A. Elabd, K. I. Winey, *Macromolecules*, **2013**, *46*, 5290. (b) Y. Ye, J.-H. Choi, K. I. Winey, Y. A. Elabd, *Macromolecules*, **2012**, *45*, 7027.
47. (a) V. F. Scalfani, E. F. Wiesenauer, J. R. Ekblad, J. P. Edwards, D. L. Gin, T. S. Bailey, *Macromolecules*, **2012**, *45*, 4262. (b) E. F. Wiesenauer, J. P. Edwards, V. F. Scalfani, T. S. Bailey, D. L. Gin, *Macromolecules*, **2011**, *44*, 5075.
48. R. L. Weber, Y. Ye, A. L. Schmitt, S. M. Banik, Y. A. Elabd, M. K. Mahanthappa, *Macromolecules*, **2011**, *44*, 5727.
49. M. Yoshizawa, M. Hirao, K. Ito-Akita, H. Ohno, *J. Mater. Chem*., **2001**, *11*, 1057.
50. (a) M. Yoshizawa, H. Ohno, *Chem. Commun*., **2004**, 1828. (b) M. Yoshizawa, A. Narita, H. Ohno, *Aust. J. Chem.*, **2004**, *57*, 139. (c) A. Narita, W. Shibayama, H. Ohno, *J. Mater. Chem*., **2006**, *16*, 1475. (d) A. Narita, W. Shibayama, M. Tamada, H. Ohno, *Polym. Bull*., **2006**, *57*, 115. (e) A. Narita, W Shibayama, K. Sakamoto, T. Mizumo, N. Matsumi, H. Ohno, *Chem. Commun.*, **2006**,

1926. (f) M. Yoshizawa-Fujita, N. Byrne, M. Forsyth, D. R. MacFarlane, H. Ohno, *J. Phys. Chem. B*, **2010**, *114*, 16373.

51. (a) N. Byrne, D. R. MacFarlane, M. Forsyth, *Electrochim. Acta*, **2005**, *50*, 3917. (b) N. Byrne, P. C. Howlett, D. R. MacFarlane, M. Forsyth, *Adv. Mater*., **2005**, *17*, 2497. (c) N. Byrnea, P. C. Howlett, D. R. MacFarlane, M. E. Smithc, A. Howesc, A. F. Hollenkampd, T. Bastowe, P. Halef, M. Forsyth, *J. Power Sources*, **2008**, *184*, 288.
52. C. Tiyapiboonchaiya, J. M. Pringle, J. Sun, N. Byrne, P. C. Howlett, D. R. Macfarlane, M. Forsyth, *Nat. Mater*., **2004**, *3*, 29.
53. (a) T. Wu, F. L. Beyer, R. H. Brown, R. B. Moore, T. E. Long *Macromolecules*, **2011**, *44*, 8056. (b) T. Wu, D. Wang, M. Zhang, J. R. Heflin, R. B. Moore, T. E. Long, *ACS Appl. Mater. Interfaces*, **2012**, *4*, 6552.

Chapter 2

Nanosegregated Assemblies of Zwitterions through the Introduction of Liquid-Crystalline Properties

Chapter 2

2-1 Introduction

Ionic liquid crystals organize into a variety of well-ordered nanoarchitectures via nanosegregation between their ionophilic and ionophobic parts.[1] There has been growing attention on their application in various fields, such as separation membranes, reaction media, and transporting materials.[2] Control of self-assembling behavior of ionic liquid crystals is required to accelerate the development of their applications because they show structure-dependent properties. It is known that liquid-crystalline (LC) phase behavior varies depending on the molecular structure and intermolecular interactions. Electrostatic interactions are an especially important driving force to control the self-assembling ability, and therefore LC phase behavior has been tuned by the selection of anion species.[3] In this context, the author expected that the use of zwitterions in the design of ionic liquid crystals would be useful for achieving control of their LC phase behavior. Previously, we found that zwitterions, such as imidazolium and phosphonium-based zwitterions, have an ability to form homogeneous mixtures with some acids or salts. It is noteworthy that physicochemical properties of zwitterions drastically change upon the addition of acids or lithium salts.[4] These property changes depend on the anion species of the additives. For example, the glass transition temperature (T_g) of an equimolar mixture of 1-ethyl-3-sulfopropylimidazolium betaine and lithium bis(trifluoromethanesulfonyl)imide ($LiTf_2N$) is -16 °C, while that of LiCl complex is 4 °C. It results from the strength of electrostatic interaction in the complexes. Then the author considered that zwitterionization of ionic liquid crystals would lead to the development of LC materials whose self-organization behavior could be tuned by the adequate selection of adding acids or salts species. In this chapter, a series of amphiphilic pyridinium-based zwitterions were designed and synthesized, and their self-organization behavior was investigated in the absence/presence of lithium salts or acids. Ionic conductivities of the obtained LC materials were also given to discuss the effects of the introduction of self-organizing properties into zwitterions and the effect on their material properties.

2-2 Results and Discussion

2-2-1 Molecular Design

The author synthesized a series of rod-shaped pyridinium-based amphiphilic zwitterions, ZI-*n*, composed of a zwitterionic part and a long alkyl chain (Figure 2-1). The author introduced an amide linkage to connect the incompatible parts because amide linkages were known to induce and stabilize the LC phases.[5] Their synthesis was performed according to the literature.[6] The index *n* indicates the number of carbon atoms in the long alkyl chain.

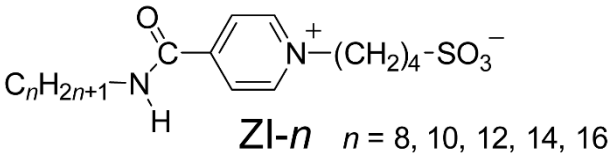

Figure 2-1. Molecular structure of pyridinium-based amphiphilic zwitterions ZI-*n*.

The LC phase behavior of ZI-*n* was investigated by differential scanning calorimetry (DSC), polarized optical microscopy (POM), and X-ray diffraction (XRD) measurements. Figure 2-2 shows the LC phase behavior of ZI-*n*, which exhibited smectic (Sm) phases from approximately 100 °C upon heating. The elongation of the alkyl chain length stabilized the LC phases. One of the driving forces for the formation of the LC phases is the nanosegregation between the ionophilic zwitterionic part and ionophobic long alkyl chains. Previously, Seddon et al. reported the phase behavior of 1-alkyl-3-methylimidazolium tetrafluoroborate with an alkyl chain (C_nH_{2n+1}: n = 0 to 18).[7] While imidazolium salts with alkyl chains $n \geq 12$ exhibited LC phases, the ones with $n \leq 11$ did not show LC properties. Instead, the series of amphiphilic zwitterions synthesized here showed LC properties, even though some of them possessed shorter alkyl chain lengths, such as ZI-8 and ZI-10. This is attributed to the strong electrostatic interactions formed between the zwitterionic headgroups of ZI-*n*, which would stabilize the molecular packing of ZI-*n*, leading to the stabilization of the LC phases. Figure 2-3 shows the POM image and XRD pattern of ZI-12.

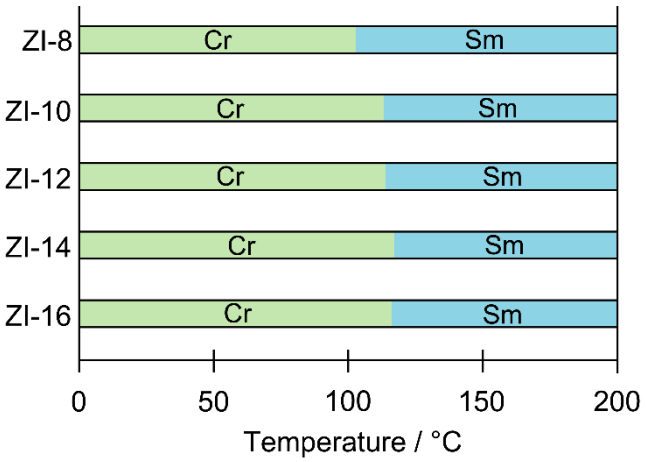

Figure 2-2. Thermotropic LC behavior of ZI-*n* on heating. Cr, crystalline; Sm, smectic.

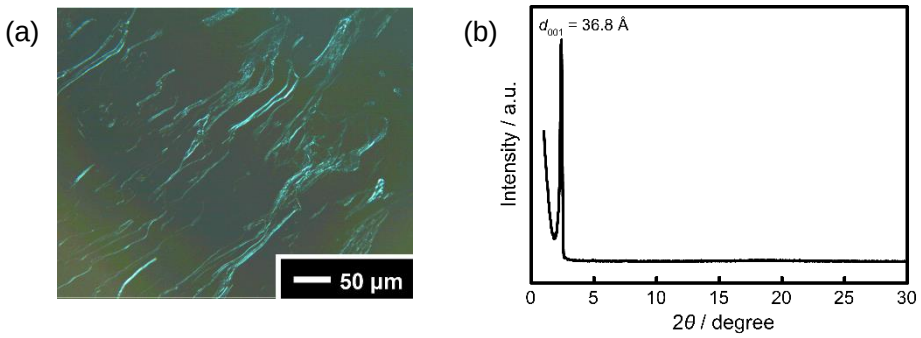

Figure 2-3. (a) POM image of ZI-12 in the Sm phase at 200 °C and (b) XRD pattern of ZI-12 in the Sm phase at 210 °C.

2-2-2 Effect of Lithium Salt Addition on the Liquid-Crystalline Properties

ZI-*n* were mixed with various lithium salts (LiX, X = Cl, BF_4, CF_3SO_3, and Tf_2N). Homogeneous mixtures of ZI-*n* and these lithium salts were prepared through slow evaporation of the methanol solution of the corresponding two components. The phase transition behavior of the equimolar mixtures of ZI-12 and LiX is summarized in Figure 2-4. Figure 2-4 clearly shows that ZI-12 shows glass transition behavior in the presence of LiX, while pristine ZI-12 undergoes crystallization. Among these LiX, addition of $LiTf_2N$ showed the largest effect on lowering of crystallinity of ZI-12. The glass transition behavior of ZI-12/$LiTf_2N$ mixture was observed at 40 °C on heating, which was about 50 °C lower than that observed for ZI-12/LiCl mixture. It is well known that the use of soft anions, such as Tf_2N anion, is effective to lower the T_g of the corresponding salts,[8] while hard anions, such as Cl anion, provide organic salts with high crystallinity. Therefore, the thermal behavior of ZI-*n*/LiX mixtures depended on the anion species of LiX, which was a similar trend to that observed for ionic liquids. These results suggest that the cationic site of ZI-*n* and the anion of the added lithium salt form ionic liquid-like ion pairs.

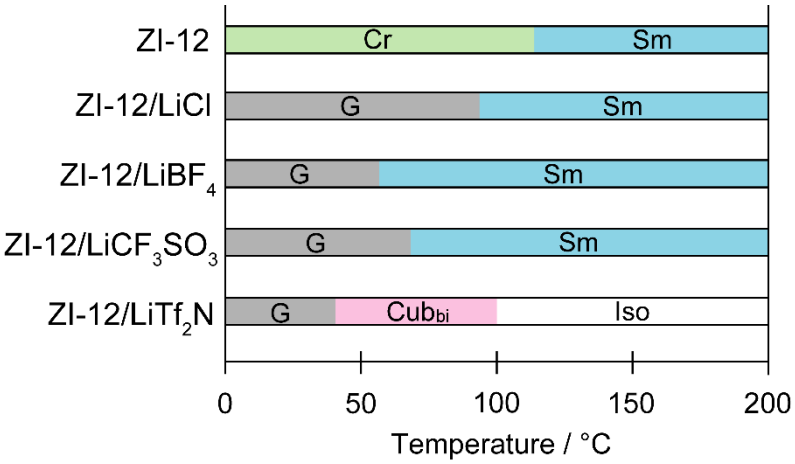

Figure 2-4. Thermotropic LC behavior of ZI-12/LiX mixtures (X = Cl, BF_4, CF_3SO_3, Tf_2N) on heating. G, glassy; Sm, smectic; Cub_{bi}, bicontinuous cubic; Iso, isotropic.

The addition of lithium salts also induced changes to the mesophase patterns. For example, ZI-12 exhibited a Sm phase with *d*-spacing of 36.8 Å, while ZI-12/$LiBF_4$ mixture formed a Sm phase with *d*-spacing of 42.0 Å (Figure 2-5). The added lithium salt would penetrate the aligned zwitterionic headgroups of ZI-12, therefore the electrostatic interactions between the zwitterionic headgroups were weakened, which led to the expansion of the ionophilic layer of the Sm phases. It is noteworthy that the mesophase patterns varied depending on the anion species of the added lithium salts. For example, the bicontinuous cubic (Cub_{bi}) phase was observed for only ZI-12/$LiTf_2N$ mixture. These results suggest that the softness of the added anions plays an important role for controlling the mesophase patterns of the amphiphilic zwitterions.

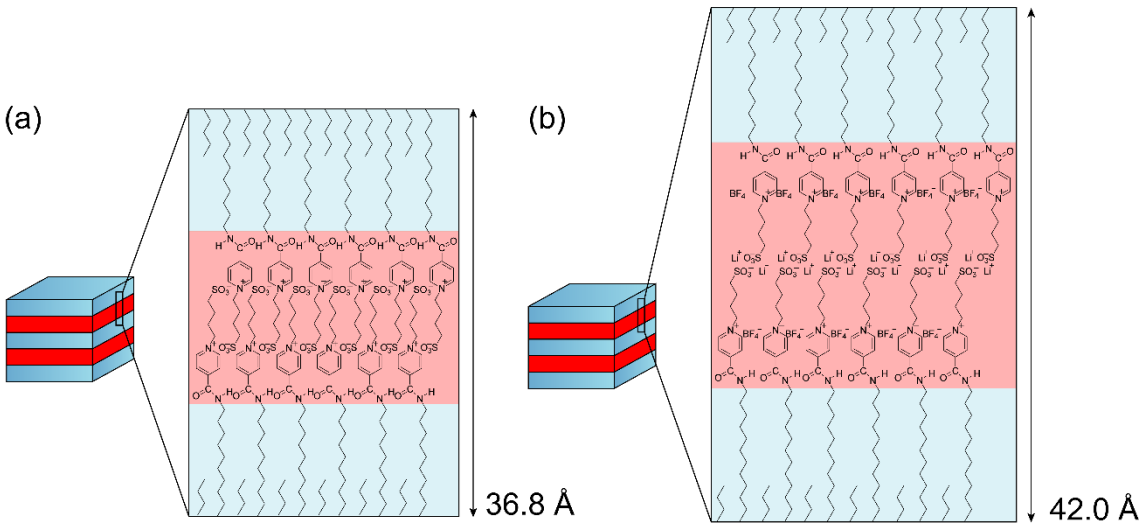

Figure 2-5. Schematic illustrations of the Sm phases formed by (a) ZI-12 and (b) ZI-12/$LiBF_4$ mixture.

There are two types of Cub_{bi} phases, i.e., direct-type and inverted-type. The former consists of 3D interconnected ionophobic nanochannel domains and an ionophilic sheath domain. The latter has the inverse structure to that of the former. Although X-ray study is a powerful method to examine the nano-ordered periodic structure, we cannot determine if the obtained Cub_{bi} phase is direct or inverted with only the X-ray results. To distinguish Cub_{bi} phases, the phase behavior of analogous compounds is generally compared by changing the hydrophobicity, e.g., using those with alkyl chains of different length.[9] Figure 2-6 summarizes the phase behavior of ZI-*n*/$LiTf_2N$ mixtures. These results clearly showed that the elongation of the alkyl chain induced mesophase pattern changes from the Cub_{bi} to Sm phase. Considering the general sequence of mesophase patterns observed for nanosegregated liquid crystals (Figure 2-7),[10] it was confirmed that the Cub_{bi} phase formed by ZI-*n*/$LiTf_2N$ mixtures should be direct Cub_{bi} phases where the zwitterionic headgroups sit on a 3D continuous gyroid minimal surface. Formation of the curved interface in the Cub_{bi} structures is attributed to the following two competitive effects. One is the hydrogen bonding among the amide groups that also effectively maintains the molecular distance between adjacent amphiphilic zwitterions. The other is the electrostatic interactions between the pyridinium cation and Tf_2N anion, which lower the T_g through the formation of ionic liquid environment by the coupling of the pyridinium cation and Tf_2N anion. This helps to expand the distance between adjacent zwitterionic headgroups.

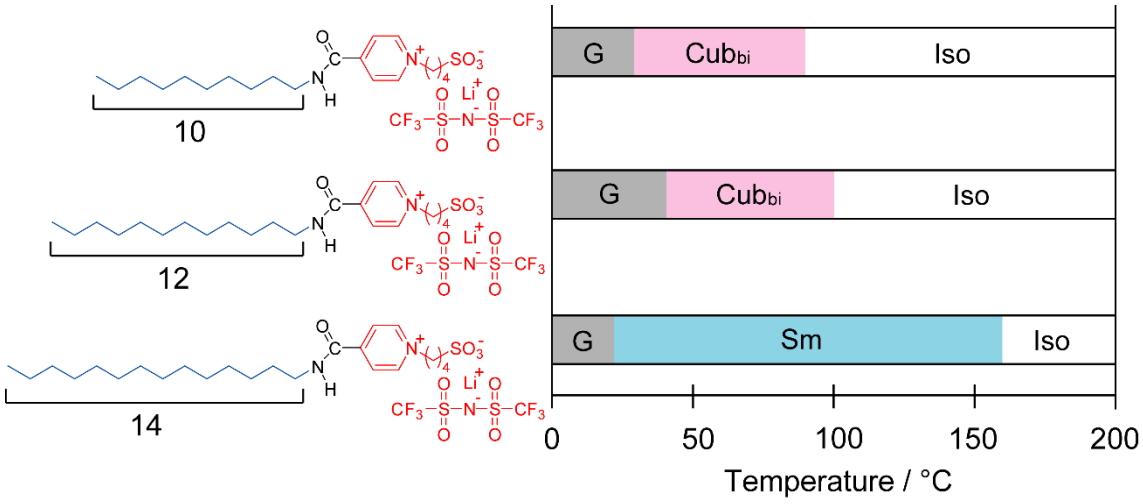

Figure 2-6. Thermotropic LC behavior of ZI-*n*/$LiTf_2N$ mixtures. G, glassy; Cub_{bi}, bicontinuous cubic; Sm, smectic; Iso, isotropic.

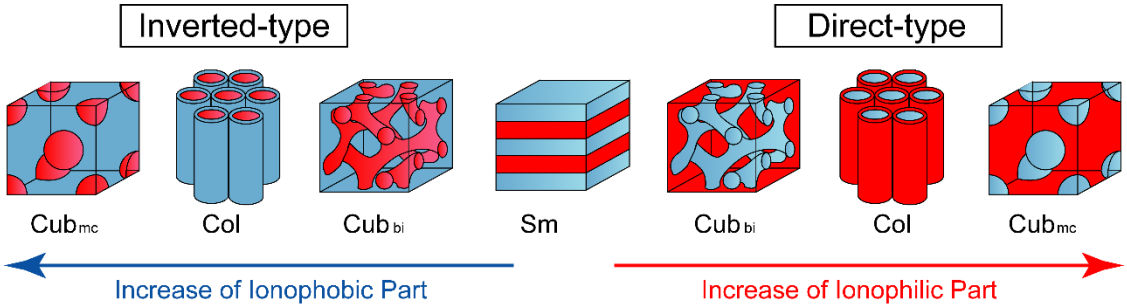

Figure 2-7. General sequence of nanosegregated liquid crystals. $Cub_{mc,}$ micellar cubic; Col, columnar; Cub_{bi}, bicontinuous cubic; Sm, smectic.

To confirm the preferential interaction between the pyridinium cation of ZI-*n* and the anion of LiX, the author applied Raman spectroscopic measurement. Since Raman spectroscopy is a powerful tool to examine the states of ions, it has been frequently employed to analyze the ion state of ionic liquids.[11] Figure 2-8 shows the Raman spectra of pristine ZI-12, $LiTf_2N$, and ZI-12/$LiTf_2N$ mixture. As a reference, a Raman spectrum of 1-ethylpyridinium bis(trifluoromethanelsulfonyl)imide ($[C_2Py][Tf_2N]$) was also analyzed. No Raman bands were observed for pristine ZI-12 in the region ranging from 800 to 650 cm^{-1}. On the other hand, $LiTf_2N$ showed a Raman band at 747 cm^{-1}, which was assigned to the symmetric bending vibration of the CF_3 group ($\delta_s(CF_3)$) of the Tf_2N anion. The $\delta_s(CF_3)$ band of the Tf_2N anion shifted to 742 cm^{-1} by the addition of ZI-12, which was approximately the same position as that of $[C_2Py][Tf_2N]$. These results lead us to conclude that, in ZI-12/$LiTf_2N$ system, the Tf_2N anion preferentially interacts with the cationic site of ZI-12 forming ion pairs with similar characteristics to those of pyridinium-type ionic liquids.

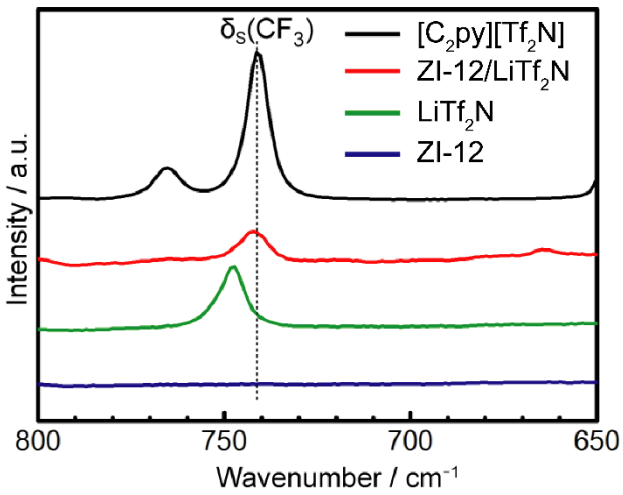

Figure 2-8. Raman spectra of pristine ZI-12, $LiTf_2N$ and ZI-12/$LiTf_2N$ mixture at 70 °C. For comparison, that of $[C_2Py][Tf_2N]$ is also shown.

The above mentioned results were useful to understand the difference in LC phase behavior of these mixtures depending on the added lithium salt species (Figure 2-9). It is known that amphiphiles with a circular cone molecular shape prefer to form a Cub_{bi} phase, while those with a cylindrical molecular shape prefer to form a layered assembly.[12] According to this general insight, the author considered that the soft and large anions of the added lithium salt would induce the circular cone structure that is suitable for the formation of Cub_{bi} phases, whereas hard anions do to form Sm phases.

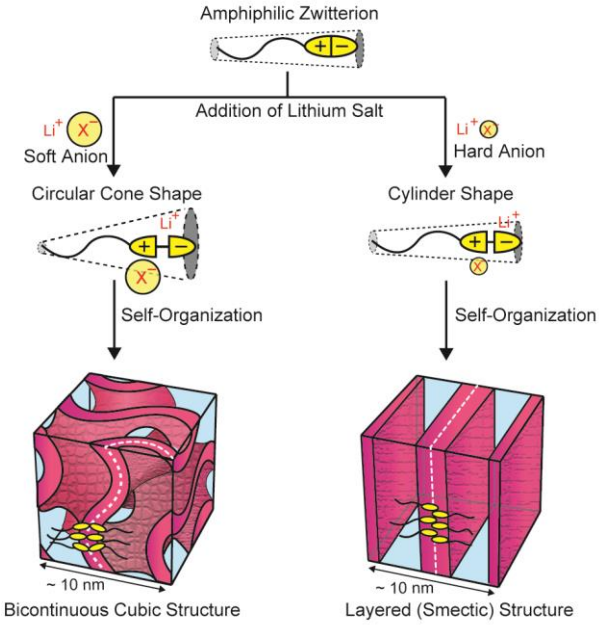

Figure 2-9. Schematic illustration that explains the induction of Cub_{bi} and Sm phases as the addition of lithium salts.

From the viewpoint mentioned above, the interface curvature of LC phases formed by amphiphilic zwitterions was considered to be controlled, not only by the selection of salt species, but also by the quantity of the adding lithium salts. The effect of the mixing ratio on the thermotropic LC behavior of ZI-12/$LiTf_2N$ mixtures is summarized as a phase diagram shown in Figure 2-10(a). Formation of the Cub_{bi} phase was confirmed to be induced when the molar ratio of $LiTf_2N$ to ZI-12 was above 0.8. With the increase of the molar ratio of $LiTf_2N$, i.e., the increase of the number of preferential ion pairs of the pyridinium cation and Tf_2N anion, a flat interface between the nanosegregated domains was progressively distorted. Consequently, the most preferential mesophase changed from layered Sm to the Cub_{bi} phase with curved intermolecular interfaces. Figure 2-10(a) clearly shows that both the T_g and isotropization temperature of the mixtures decreased as the molar ratio of $LiTf_2N$ increased. These are also comprehensible as the effect of ionic liquid-like environment formed by the pyridinium cation

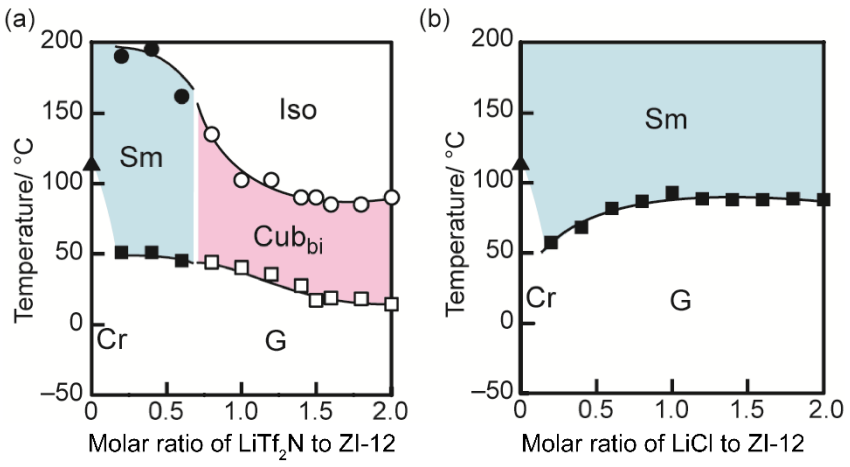

Figure 2-10. Phase diagrams of (a) ZI-12/LiTf$_2$N mixtures and (b) ZI-12/LiCl mixtures on heating. Cr, crystalline; G, glassy; Sm, smectic; Cub$_{bi}$, bicontinuous cubic; Iso, isotropic.

and Tf$_2$N anion. In contrast to the case of ZI-12/LiTf$_2$N mixtures, mesophase change was not observed for ZI-12/LiCl mixtures as shown in Figure 2-10(b). Comparison of the two phase diagrams also supports the idea that the selection of LiX is important for controlling the curvature of the intermolecular interface formed by the zwitterionic parts.

The mesophase patterns of ZI-*n*/LiX mixtures were characterized by POM observation and XRD measurements. For example, under cross-Nicol condition, the ZI-12/LiTf$_2$N mixture in a 5:3 molar ratio showed an oily streak texture at 120 °C (Figure 2-11(a)). The XRD pattern of the mixture at 100 °C showed four intense peaks at 38.7, 18.9, 12.5, and 9.3 Å in a small-angle region (Figure 2-11(b)). The reciprocal *d*-spacing ratio of the four peaks is 1:2:3:4, which can be attributed to the formation of a Sm phase. On the other hand, the ZI-12/LiTf$_2$N mixture in a 2:3 molar ratio showed no birefringence at 60 °C (Figure 2-12(a)). The XRD pattern of the mixture at 60 °C shows two intense peaks at 38.3 and 33.6 Å in the small-angle region (Figure 2-12(b)). The reciprocal *d*-spacing ratio of the two peaks is $\sqrt{6}$:$\sqrt{8}$, which can be assigned to the (211) and (220) reflections of Cub$_{bi}$ structures with *Ia*3*d* symmetry.

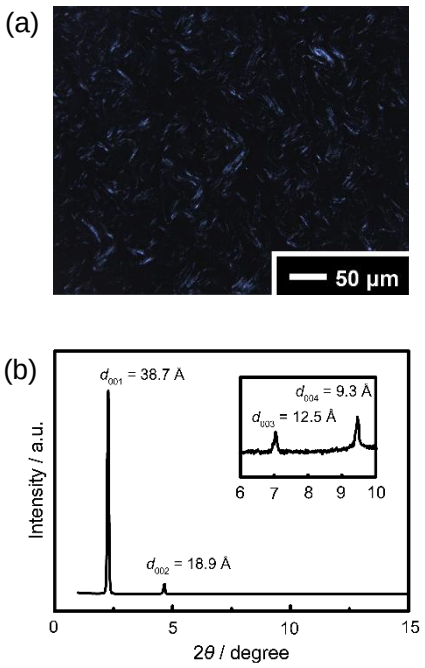

Figure 2-11. (a) POM image of ZI-12/$LiTf_2N$ mixture in a 5:3 molar ratio in the Sm phase at 120 °C. (b) XRD pattern of ZI-12/$LiTf_2N$ mixture in a 5:3 molar ratio in the Sm phase at 100 °C.

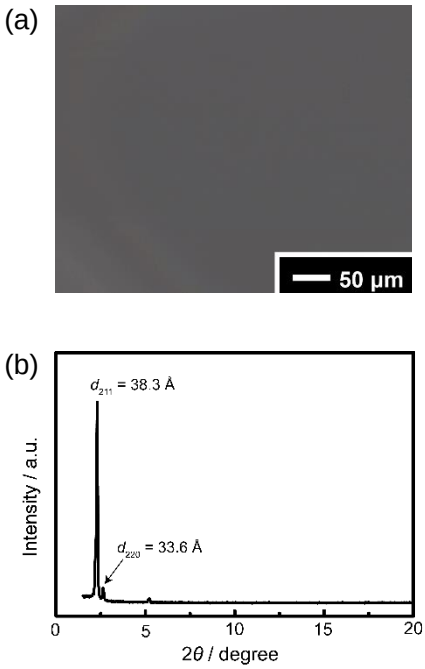

Figure 2-12. (a) POM image of ZI-12/$LiTf_2N$ mixture in a 2:3 molar ratio in the Cub_{bi} phase at 60 °C. (b) XRD pattern of ZI-12/$LiTf_2N$ mixture in a 2:3 molar ratio in the Cub_{bi} phase at 60 °C.

2-2-3 Effect of Acid Addition on the Liquid-Crystalline Properties

To confirm the effect of acid addition on the self-assembling behavior of the amphiphilic zwitterions, as well as that of lithium salts, we also mixed ZI-*n* with HTf_2N, and then the LC phase behavior of the obtained mixtures was investigated. As well as lithium salts, addition of HTf_2N to ZI-12 induced the mesophase pattern changes. Figure 2-13 summarizes LC properties of ZI-*n*/HTf_2N mixtures. These mixtures exhibited columnar (Col) and Cub_{bi} phases depending on the alkyl chain length, *n*, while pristine ZI-*n* formed only Sm phases. For example, ZI-12/HTf_2N mixture exhibited a Col phase from 66 °C on cooling and partially underwent a phase transition to a Cub_{bi} phase at around 58 °C as shown in Figure 2-14, while ZI-14/HTf_2N mixture showed only a Cub_{bi} phase from 32 to 105 °C on heating. These results suggest that the acid addition is also effective for controlling the self-assembly ability of the amphiphilic zwitterions.

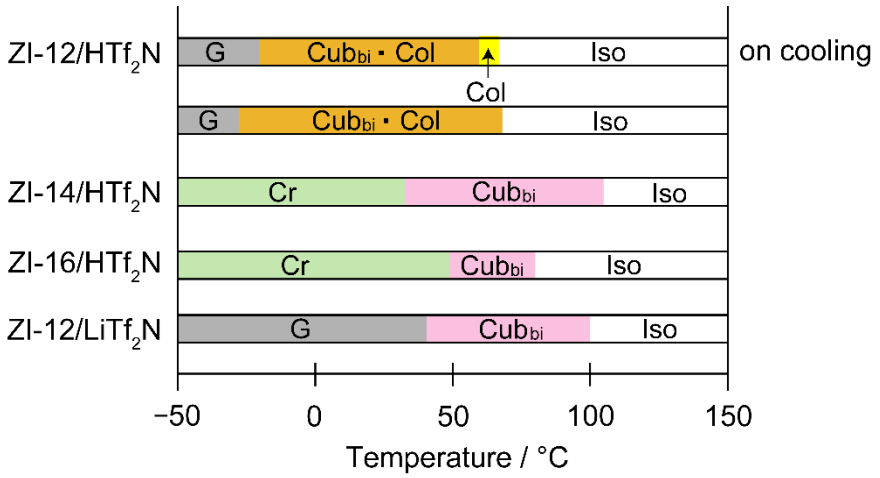

Figure 2-13. Thermotropic LC behavior of ZI-*n*/HTf$_2$N mixtures (*n* = 12, 14, 16) and ZI-12/LiTf$_2$N mixture on heating. Cr, crystalline; G, glassy; Sm, smectic; Col, columnar; Cub$_{bi}$, bicontinuous cubic; Iso, isotropic.

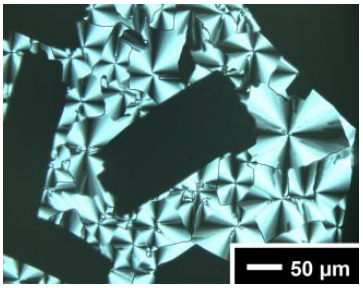

Figure 2-14. POM image of ZI-12/HTf$_2$N mixture at the phase transition from the Col to Cub$_{bi}$ phase on cooling.

Characterization of mesophase patterns was performed with XRD measurements. The XRD pattern of ZI-12/HTf$_2$N mixture showed two peaks at 36.7 and 18.2 Å in the small-angle region (Figure 2-15(a)). The reciprocal *d*-spacing ratio of these two peaks was 1:2, which should be assigned to (001) and (002) reflections of a Col structure, respectively. On the other hand, the XRD pattern of ZI-16/HTf$_2$N mixture at 60 °C showed two intense peaks at 42.4 and 36.6 Å, as seen in Figure 2-15(b). The ratio of reciprocal *d*-spacing of two peaks was assigned to (211) and (220) reflections of a Cub$_{bi}$ structure with *Ia*3*d* symmetry, respectively.

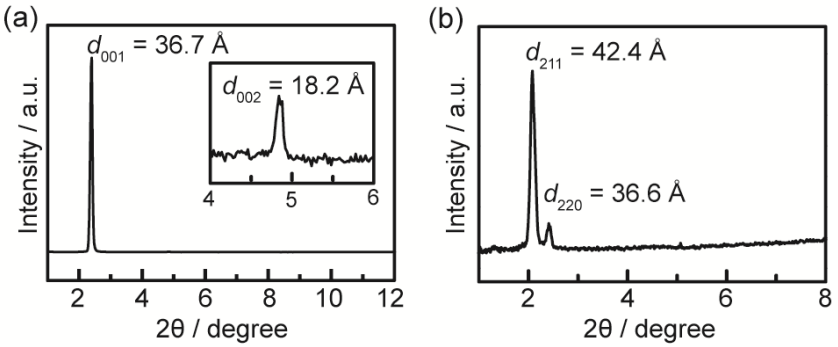

Figure 2-15. XRD patterns of (a) ZI-12/HTf_2N mixture in the Col phase at 60 °C and (b) ZI-16/HTf_2N mixture in the Cub_{bi} phase at 60 °C.

In the above section, the author described that the addition of acids or salts containing soft anion, such as Tf_2N, is effective for inducing amphiphilic zwitterions to form Cub_{bi} phases. In the Cub_{bi} phases, the periphery of the long alkyl chain of ZI-*n* is located in the center of 3D continuous nanochannel domains and the other end of the amphiphilic molecule, the sulfonate anion and proton or lithium ion, sits on a gyroid minimal surface that separates the nanochannel domains in middle of the structure. To examine the potential utility of the gyroid minimal surface for a continuous interface, the author examined the mobility of ions in the materials using alternative current impedance method. Figure 2-16 shows the ionic conductivity of ZI-14/HTf_2N mixture containing a small amount of water. These LC materials showed high ionic conductivity when they formed Cub_{bi} phases and then their conductivity drastically decreased upon phase transition from the Cub_{bi} to isotropic liquid phase. For example, the ionic conductivity of ZI-14/HTf_2N mixture containing 1.4 wt% of water in the Cub_{bi} phase at 98 °C is 8.4×10^{-5} S cm^{-1}, which is about 3 times higher than that in the isotropic state at 136 °C. The mobility of ions in LC materials is generally governed by the local environment of ions and the macroscopic continuity of ion conductive pathways.[2(a)] Taking this general insight into account, the author attributed the effective ion conduction behavior in the Cub_{bi} phases to the formation of a macroscopically continuous ion conductive pathway. Namely, the zwitterionic parts sitting on a 3D continuous gyroid minimal surface form a successive ion conductive pathway. This maintains continuity, even on the LC domain boundaries. These results strongly suggest that the use of a gyroid minimal surface is a potential strategy for the construction of a macroscopically continuous interface that would not require alignment control.

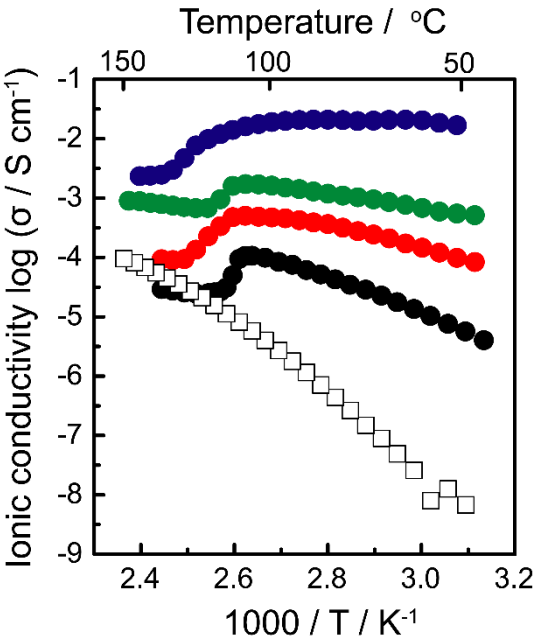

Figure 2-16. Ionic conductivities of ZI-14/HTf_2N mixtures containing 1.4 wt% (●), 6.1 wt% (●), 7.3 wt% (●), and 8.9 wt% (●) of water and ZI-12/$LiTf_2N$ mixture (□) on heating.

To obtain further insight into ion conduction behavior of these materials, the author prepared ZI-14/HTf_2N mixtures with various water contents and examined their ion conduction behavior. With the increase of water content, the ionic conductivities of the samples increased while the activation energy for ion conduction estimated from Arrhenius plots decreased. These results can be explained by the changes of ion conduction mechanism that mainly governs the proton conduction behavior of the present materials. It is well known that there are two types of ion conduction mechanisms. One is vehicle mechanism and the other is hopping (Grotthuss) mechanism. In vehicle mechanism, protons are transported via self-diffusion, which requires a high activation energy, while in hopping mechanism protons are transported via hydrogen bonding network, which requires a low activation energy. Considering this, in the present systems, protons were transported through the hydrogen bonding network along the gyroid minimal surface via hopping mechanism.

The ionic conductivity of ZI-12/$LiTf_2N$ that formed a Cub_{bi} phase was also measured. The ionic conductivity of ZI-12/$LiTf_2N$ linearly increased beyond the phase transition temperature from the Cub_{bi} to isotropic state. Considering that the lithium ion conduction is mainly dominated by vehicle mechanism, the carrier ions, lithium cations and Tf_2N anions, would migrate via self-diffusion in a 3D connected zwitterionic domain. The obtained results suggest that in the present system, the gyroid minimal surface plays an essential role as ion conductive matrix especially for protons.

2-2-4 Effect of Ionic Liquid Addition on the Liquid-Crystalline Properties

Recently, various unique properties of ionic liquids[13] has increased the attention toward lyotropic LC systems containing ionic liquids as self-organization media.[14] It has been gradually revealed that self-assembly behavior of amphiphiles in ionic liquids is different from that in conventional solvents, such as water. Herein, the author demonstrates the potential utility of the zwitterionic structure as the ionophilic moiety for the design of amphiphiles in ionic liquids. It is interesting that ZI-*n*/HTf$_2$N mixture showed lyotropic LC behavior in the presence of some protic ionic liquids. For example, 1H,3H-imidazolium bis(trifluoromethanesulfonyl) imide ([HIm][Tf$_2$N]) was easily prepared by mixing imidazole with an equimolar amount of bis(trifluoromethanesulfonyl)imide acid. The addition of [HIm][Tf$_2$N] to ZI-*n*/HTf$_2$N mixture induced lyotropic LC behavior. For example, ZI-16/HTf$_2$N mixture containing 12.1 wt% [HIm][Tf$_2$N] formed a Cub$_{bi}$ phase from 42 to 95 °C on cooling. Further addition of [HIm][Tf$_2$N] to ZI-16/HTf$_2$N mixture induced the Col phase. A phase diagram of ZI-16/HTf$_2$N mixture in the presence of [HIm][Tf$_2$N] is shown in Figure 2-17. The induced mesophases and their temperature ranges changed depending on the amount of protic ionic liquids. The phase sequence observed here accords to that of conventional lyotropic LC systems. These results suggest that the material design based on the combination of amphiphilic zwitterions and protic ionic liquids is useful for the development of ionic liquid-based lyotropic LC systems.

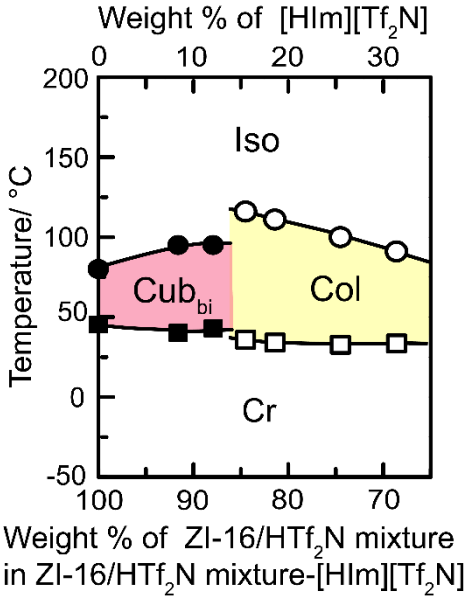

Figure 2-17. Lyotropic LC behavior of ZI-16/HTf$_2$N mixture containing [HIm][Tf$_2$N] as solvent. The phase transition temperatures were determined on cooling. Cr, crystalline; G, glassy; Cub$_{bi}$, bicontinuous cubic; Col, columnar; Iso, isotropic.

The characterization of mesophase patterns was performed by POM observation and XRD measurement. The POM image of ZI-16/HTf_2N mixture containing 12.1 wt% [HIm][Tf_2N] showed no birefringence, which is attributed to the formation of an isotropic state (Figure 2-18). The XRD pattern of ZI-16/HTf_2N mixture containing 12.1 wt% [HIm][Tf_2N] showed two peaks in a small angle region. The reciprocal *d*-spacing ratio of these two peaks is $\sqrt{6}:\sqrt{8}$, which can be assigned to the (211) and (220) reflections of a Cub_{bi} structure. The POM image of ZI-16/HTf_2N mixture containing 18.6 wt% [HIm][Tf_2N] showed a focal conic fan texture, which is characteristic for a Col structure (Figure 2-19). The XRD pattern of ZI-16/HTf_2N mixture containing 18.6 wt% [HIm][Tf_2N] showed two peaks. The reciprocal *d*-spacing ratio of these two peaks is 1:2, which should be assigned to (001) and (002) reflections of a Col structure.

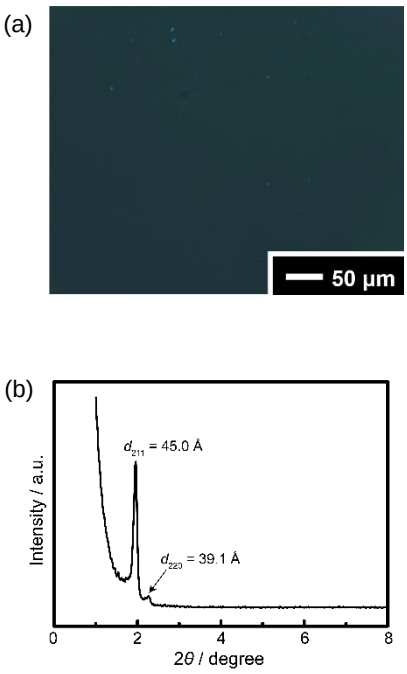

Figure 2-18. (a) POM image of ZI-16/HTf_2N mixture containing 12.1 wt% of [HIm][Tf_2N] in the Cub_{bi} phase at 60 °C. (b) XRD pattern of ZI-16/HTf_2N mixture containing 12.1 wt% of [HIm][Tf_2N] in the Cub_{bi} phase at 60 °C.

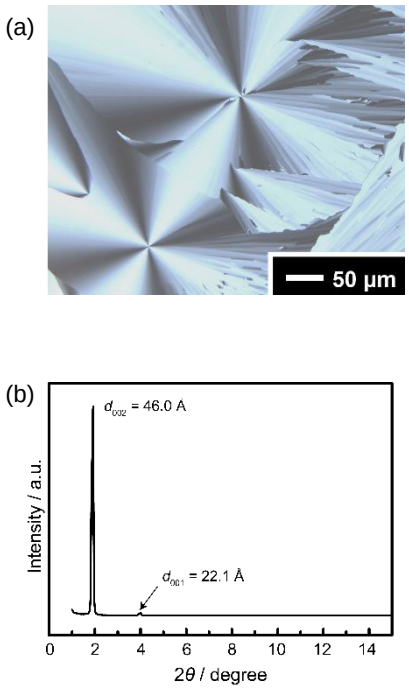

Figure 2-19. (a) POM image of ZI-16/HTf_2N mixture containing 18.6 wt% of [HIm][Tf_2N] in the Col phase at 60 °C. (b) XRD pattern of ZI-16/HTf_2N mixture containing 18.6 wt% of [HIm][Tf_2N] in the Col phase at 60 °C.

2-3 Conclusion

The author examined the effects of the addition of various lithium salts on the LC phase behavior of pyridinium-based amphiphilic zwitterions. The changes of mesophase patterns were observed upon the addition of lithium salts, and the observed mesophase patterns depended on the anion species of the additives. In particular, the addition of lithium salts having soft anions, such as Tf_2N anion, was effective for the induction of nanosegregated aggregates with a curved interface, such as Cub_{bi} phases. The exhibition of Cub_{bi} phases was also induced by the addition of an acid containing the Tf_2N anion. Raman spectroscopy revealed that the pyridinium cations preferred to interact with the Tf_2N anions. These results strongly suggest that the formation of a preferential ion pair expands the distance between the adjacent zwitterionic headgroups, leading to the formation of a curved interface. Ion conductivity measurement revealed that the gyroid minimal surface of obtained Cub_{bi} assemblies formed a continuously connected monodomain transporting ions.

2-4 Experimental

General Procedures

^1H NMR and ^{13}C NMR spectra were obtained on a JEOL NMR spectrometer (α-400). Chemical shifts of ^1H and ^{13}C signals were quoted to $(CH_3)_4Si$ (δ = 0.00) and $CDCl_3$ (δ= 77.0) as internal standards, respectively. Elemental analysis was carried out on an Elementar Analytical vario EL3. Thermal properties of the materials were examined with a DSC using DSC-6220, Seiko Instruments. Heating and cooling rate was 5 °C min^{-1}. A polarizing optical microscope, Olympus BX51 equipped with a Lincam hot-stage, was used for observation of LC phases. XRD patterns were obtained using a Rigaku RINT-2500 diffractometer with CuKα radiation. The Raman spectra were obtained using a JASCO NRS-1000 spectrometer with a Kaiser Optical holographic super-notch filter and a liquid N_2-cooled CCD detector. A Coherent Innova 90C Kr laser with a 20mW beam at a 647.1 nm excitation wavelength was used for excitation.

Materials

All chemicals were obtained from commercial sources and used without purification. All reactions were carried out under an argon atmosphere in anhydrous solvents.

Synthesis

The synthetic pathways used to obtain compounds ZI-*n* are shown in Scheme 2-1. Pyridine-4-carboxylic acid was treated with thionyl chloride to yield the corresponding carboxylic acid chloride. Then the resultant carboxylic acid chloride was reacted with 1-aminoalkane ($CH_3(CH_2)_{n-1}NH_2$, *n*:

carbon number of alkyl chain) to yield *N*-alkylisonicotinamide, Py-*n*. Subsequent quaternization reaction of Py-*n* with 1, 4-butanesultone in THF gave pyridinium-based zwitterions ZI-*n*.

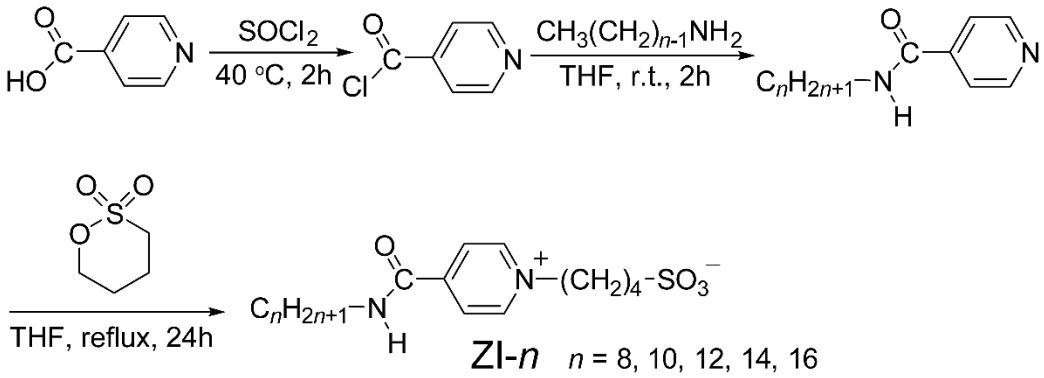

Scheme 2-1. Synthesis of pyridinium-based amphiphilic zwitterion (ZI-*n*).

<u>*N*-dodecylcarbamoyl-pyridine (Py-12)</u>

Isonicotinic acid (4.1g; 33.3 mmol) was converted into the corresponding acid chloride by stirring in 20 ml of thionyl chloride at 40 °C for 2 h. The reactant was precipitated as a white solid through the addition of an excessive amount of hexane (50 ml) and the resultant white precipitate was washed three times with cold hexane. A solution of dodecylamine (5.6 g; 30.2 mmol) and pyridine (5.0 g; 63.2 mmol) in THF (40 mL) was added dropwise to the acid chloride with stirring at 0 °C. The mixture was stirred at room temperature for 2 h. Then water and ethyl acetate were added, the organic layer was separated and washed with water. The resulting organic phase was dried over anhydrous $MgSO_4$. The insoluble materials were filtered off through filter paper. The filtrate was concentrated by rotary evaporation. The crude product was purified by flash column chromatography (silica gel, eluent: chloroform/MeOH = 20/1). The crude product was recrystallized from ethylacetate to give Py-12 (6.9 g; 23.7 mmol; 71 %) as a white solid.

^{1}H NMR (400 MHz, $CDCl_3$): δ = 8.73 (m, 2H), 7.59 (m, 2H), 6.21 (s, 1H), 3.47 (m, 2H), 1.65 (m, 2H), 1.36-1.26 (m, 18H), 0.88 (t, *J* = 7.33 Hz, 3H). ^{13}C NMR (400 MHz, $CDCl_3$): δ = 165.48, 150.52, 141.89, 120.80, 40.27, 31.87, 30.90, 29.59, 29.54, 29.49, 29.31, 29.25, 26.93, 22.65, 14.08.

dodecylcarbamoyl-1-(4-sulfobutyl)-pyridinium betaine (ZI-12)

1, 4-butane sultone (3.3 g, 24.2 mmol) was added to a solution of Py-12 (3.0 g, 10.3 mmol) in THF (50 mL) with stirring at room temperature. The mixture was refluxed for 24 h. Through recrystallization from chloroform/methanol mixed solvent, colorless crystal (3.2 g, 7.5 mmol) was obtained in 73 % yield.

^{1}H NMR (400 MHz, $CDCl_3$:CD_3OD =3:1): δ = 9.13 (m, 2H), 8.38 (m, 2H), 4.75 (m, 2H), 3.44 (m, 2H), 2.91 (m, 2H), 2.24 (m, 2H), 1.86 (m, 2H), 1.65 (m, 2H), 1.35-1.27 (m, 18H), 0.88 (m, 3H). ^{13}C NMR (400 MHz, $CDCl_3$:CD_3OD =3:1): δ = 161.91, 149.37, 145.18, 126.07, 61.01, 49.44, 40.49, 31.56, 29.64, 29.29, 29.26, 29.22, 28.98, 28.72, 26.68, 22.31, 20.87, 13.61. Elemental analysis. Calcd for $C_{22}H_{38}N_2O_4S$ H_2O: C, 59.43; H, 9.07; N, 6.30. Found: C, 59.37; H, 9.00; N, 6.08.

ZI-8

^{1}H NMR (400 MHz, CD_3OD): δ = 9.15 (d, *J* = 6.80 Hz, 2H), 8.39 (d, *J* = 6.80 Hz, 2H), 4.71 (t, *J* = 7.40 Hz, 2H), 3.45 (t, *J* = 7.00 Hz, 2H), 2.89 (t, *J* = 7.20 Hz, 2H), 2.21 (m, 2H), 1.83 (m, 2H), 1.65 (m, 2H), 1.37-1.30 (m, 10H), 0.90 (t, *J* = 6.80 Hz, 3H).

ZI-10

^{1}H NMR (400 MHz, CD_3OD): δ = 9.13 (d, *J* = 6.41 Hz, 2H), 8.38 (d, *J* = 6.41 Hz, 2H), 4.72 (t, *J* = 7.79 Hz, 2H), 3.43 (t, *J* = 7.33 Hz, 2H), 2.87 (m, 2H), 2.22 (m, 2H), 1.83 (m, 2H), 1.65 (m, 2H), 1.38-1.30 (m, 14H), 0.90 (t, *J* = 6.87 Hz, 3H). ^{13}C NMR (400 MHz, $CDCl_3$:CD_3OD =3:1): δ = 161.91, 149.36, 145.17, 126.07, 61.01. 49.45, 40.48, 31.52, 29.64, 29.20, 28.95, 28.72, 26.67, 22.30, 20.88, 13.59. Elemental analysis. Calcd for $C_{20}H_{34}N_2O_4S$ H_2O: C, 57.66; H, 8.71; N, 6.72. Found: C, 57.56; H, 8.59; N, 6.59.

ZI-14

^{1}H NMR (400 MHz, $CDCl_3$:CD_3OD = 3:1): δ = 9.12 (m, 2H), 8.38 (m, 2H), 4.75 (m, 2H), 3.44 (m, 2H), 2.92 (m, 2H), 2.23 (m, 2H), 1.84 (m, 2H), 1.66 (m, 2H), 1.35-1.26 (m, 22H), 0.88 (m, 3H). ^{13}C NMR (400 MHz, $CDCl_3$:CD_3OD =3:1): δ = 161.90, 149.43, 145.14, 126.07, 61.01, 49.31, 40.50, 31.57, 29.55, 29.30, 29.00, 28.74, 26.69, 22.32, 20.76, 13.61. Elemental analysis. Calcd for $C_{24}H_{42}N_2O_4S$ H_2O: C, 60.98; H, 9.38; N, 5.93. Found: C, 60.92; H, 9.44; N, 5.66.

ZI-16

^{1}H NMR (400 MHz, $CDCl_3$:CD_3OD = 3:1): δ = 9.07 (m, 2H), 8.34 (m, 2H), 4.74 (m, 2H), 3.44 (m, 2H), 2.90 (m, 2H), 2.26 (m, 2H), 1.83 (m, 2H), 1.65 (m, 2H), 1.36-1.24 (m, 26H), 0.88 (m, 3H). ^{13}C NMR (400 MHz, $CDCl_3$:CD_3OD =3:1): δ = 161.98, 149.46, 145.14, 126.07, 61.01, 49.32, 40.64, 31.57, 30.38, 29.56, 29.33, 29.23, 29.00, 28.75, 26.69, 22.32, 20.77, 13.61. Elemental analysis. Calcd for $C_{26}H_{46}N_2O_4S$ H_2O: C, 62.36; H, 9.66; N, 5.59. Found: C, 62.08; H, 9.44; N, 5.83.

2-5 References

1. (a) K. Binnemans, *Chem. Rev*., **2005**, *105*, 4148. (b) T. Kato, N. Mizoshita, K. Kishimoto, *Angew. Chem., Int. Ed*., **2006**, *45*, 38. (c) X. Cheng, X. Bai, S. Jing, H. Ebert, M. Prehm, C. Tschierske, *Chem. -Eur. J*., **2010**, *16*, 4588.
2. (a) T. Kato, *Science*, **2002**, *295*, 2414. (b) W. Dobbs, J.-M. Suisse, L. Douce, R. Welter, *Angew. Chem., Int. Ed*., **2006**, *45*, 4179. (c) Y. Zakrevskyy, J. Stumpe, C. F. J. Faul, *Adv. Mater*., **2006**, *18*, 2133. (d) D. Batra, S. Seifert, L. M. Varela, A. C. Y. Liu, M. A. Firestone, *Adv. Funct. Mater*., **2007**, *17*, 1279. (e) T. Ichikawa, M. Yoshio, A. Hamasaki, T. Mukai, H. Ohno, T. Kato, *J. Am. Chem. Soc*., **2007**, *129*, 10662. (f) M. Henmi, K. Nakatsuji, T. Ichikawa, H. Tomioka, T. Sakamoto, M. Yoshio, T. Kato, *Adv. Mater*., **2012**, *24*, 2238. (g) Y. Ishida, Y. Kai, S. Kato, A. Misawa, S. Amano, Y. Matsuoka, K. Saigo, *Angew. Chem. Int. Ed*., **2008**, *47*, 8241.
3. (a) C. J. Bowlas, D. W. Bruce, K. R. Seddon, *Chem. Commun*., **1996**, 1625. (b) D. Kim, S. Jon, H.-K. Lee, K. Baek, N.-K. Oh, W.-C. Zin, K. Kim, *Chem. Commun*., **2005**, 5509. (c) M. Yoshio, T. Ichikawa, H. Shimura, T. Kagata, A. Hamasaki, T. Mukai, H. Ohno, T. Kato, *Bull. Chem. Soc. Jpn*., **2007**, *80*, 1836. (d) P. H. J. Kouwer, T. M. Swager, *J. Am. Chem. Soc*., **2007**, *129*, 14042. (e) Y. Haketa, S. Sasaki, N. Ohta, H. Masunaga, H. Ogawa, N. Mizuno, F. Araoka, H. Takezoe, H. Maeda, *Angew. Chem. Int. Ed*., **2010**, *49*, 10079.
4. (a) M. Yoshizawa, M. Hirao, K. I. Akita, H. Ohno, *J. Mater. Chem*., **2001**, *11*, 1057. (b) M. Yoshizawa, H. Ohno, *Chem. Commun*., **2004**, 1828.
5. (a) G. Ungar, D. Abramic, V. Percec, J. A. Heck, *Liq. Cryst.*, **1996**, *21*, 73. (b) V. Percec, C.-H. Ahn, T. K. Bera, G. Ungar, D. J. P. Yeardley, *Chem. Eur. J*., **1999**, *5*, 1070.
6. (a) S. Ueda, J. Kagimoto, T. Ichikawa, T. Kato, H. Ohno, *Adv. Mater*., **2011**, *23*, 3071. (b) S. Taguchi, T. Ichikawa, T. Kato, H. Ohno, *Chem. Commun*., **2012**, *48*, 5271. (c) B. Soberats, M. Yoshio, T. Ichikawa, S. Taguchi, H. Ohno, T. Kato, *J. Am. Chem. Soc*., **2013**, *135*, 15286. (d) T. Ichikawa, T. Kato, H. Ohno, *J. Am. Chem. Soc*., **2012**, *134*, 11354.
7. J. D. Holbrey, K. R. Seddon, *J. Chem. Soc., Dalton Trans*., **1999**, 2133.
8. (a) P. Bonhôte, A.-P. Dias, N. Papageorgiou, K. Kalyanasundaram, M. Grätzel, *Inorg. Chem*., **1996**, *35*, 1168. (b) J. Sun, M. Forsyth, D. R. MacFarlane, *J. Phys. Chem. B*, **1998**, *102*, 8858.
9. (a) S. Kutsumizu, K. Morita, T. Ichikawa, S. Yano, S. Nojima, T. Yamaguchi, *Liq. Cryst*., **2002**, *29*, 1447. (b) F. Neve, M. Impéror-Clerc, *Liq. Cryst*., **2004**, *31*, 907. (c) M. Lee, Y.-S. Yoo, *J. Mater. Chem*., **2002**, *12*, 2161. (d) K. Goossens, S. Wellens, K. V. Hecke, L. V. Meervelt, T. Cardinaels, K. Binnemans, *Chem. -Eur. J*., **2011**, *17*, 4291.
10. P. Fuchs, C. Tschierske, K. Raith, K. Das, S. Diele, *Angew. Chem., Int. Ed*., **2002**, *41*, 628.
11. W. Ogihara, N. Suzuki, N. Nakamura, H. Ohno, *Polym. J*., **2006**, *38*, 117.
12. C. Tschierske, *J. Mater. Chem*., **1998**, *8*, 1485.

13. (a) T. Welton, *Chem. Rev*., **1999**, *99*, 2071. (b) J. S. Wilkes, *Green Chem*., **2002**, *4*, 73. (c) R. D. Rogers, K. R. Seddon, *Science*, **2003**, *302*, 792. (d) M. Armand, F. Endres, D. R. MacFarlane, H. Ohno, B. Scrosati, *Nat. Mater*., **2009**, *8*, 621.
14. (a) T. L. Greaves, C. J. Drummond, *Chem. Soc. Rev*., **2008**, *37*, 1709. (b) R. Atkin, G. G. Warr, *J. Am. Chem. Soc*., **2005**, *127*, 11940. (c) L. A. Robertson, M. R. Schenkel, B. R. Wiesenauer, D. L. Gin, *Chem. Commun*., **2013**, *49*, 9407. (d) T. Ichikawa, M. Yoshio, S. Taguchi, J. Kagimoto, H. Ohno, T. Kato, *Chem. Sci*., **2012**, *3*, 2001. (e) T. Ichikawa, K. Fujimura, M. Yoshio, T. Kato, H. Ohno, **2013**, *49*, 11746.

Chapter 3

Gemini Amphiphilic Zwitterions Exhibiting Nanosegregated Assemblies

Chapter 3

3-1 Introduction

The introduction of liquid-crystalline (LC) properties into ionic liquids is considered one of the potential ways to expand the functions of ionic liquids since self-organizing ionic liquids show unique properties dependent on their assembled structures. Ionic liquids crystals have become popular in various fields, including separation membranes,[1] reaction media,[2] and ion conductors.[3] To date, a number of ionic liquid crystals have been designed and synthesized to investigate the relationship between their molecular structures, assembled structures, and potential applications.[4] Gemini amphiphilic molecules are a class of LC materials consisting of two high polar headgroups tethered with covalent bonds and low polar tails. In particular, there have been studies on lyotropic LC systems. For example, they show a lower critical micelle concentration in solvents than traditional amphiphiles.[5] Although their self-organization behavior in the presence of water was studied intensively,[6] there are few reports on their thermotropic LC properties.[7] Recently, geminal structures were employed in the design of ionic liquids and showed different properties from traditional ones.[8] In this context, the author expected that the use of geminal structures into the design of thermotropic ionic LC materials would expand their potential applications. In chapter 2, the author determined that amphiphilic zwitterions showed thermotropic LC properties and their assembled states changed with the addition of acids or salts. Furthermore, it was shown that amphiphilic zwitterions showed unique ion conductive properties derived from their morphology. With this background in mind, the author envisioned that zwitterionization of ionic gemini amphiphiles would provide further understanding of self-organization behavior of thermotropic LC materials and their functions. In this chapter, the author designed and synthesized gemini zwitterionic amphiphiles with two zwitterionic headgroups tethered with a spacer and long alkyl chains and investigated their self-organization behavior.

3-2 Results and Discussion

3-2-1 Molecular Design

There are few reports on thermotropic LC gemini amphiphiles except for a few ammonium salts[9] and imidazolium salts.[7a] To examine the potential utility of gemini zwitterions as building blocks of thermotropic LC materials, the author chose imidazolium salts as a basic design because the imidazolium structure was considered to provide many opportunities for functionalization of LC materials. For example, each of the N and C position of the imidazolium ring can be selectively substituted.[7a, 10] Then, the author designed and synthesized gemini imidazolium-based amphiphilic zwitterions, ZI-*n* (*n* means the number of carbon atoms in a long alkyl chain) (Figure 3-1). They consisted of both imidazolium zwitterionic groups and long alkyl chains tethered with a covalent bond.

Their synthesis was described in section 3-4.

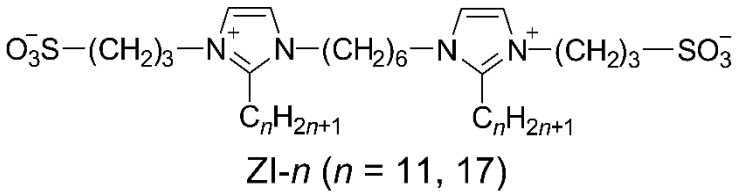

ZI-*n* (*n* = 11, 17)

Figure 3-1. Molecular structure of gemini imidazolium-based amphiphilic zwitterions (ZI-*n*).

3-2-2 Liquid-Crystalline Properties of Gemini Amphiphilic Zwitterions

Phase behavior of ZI-*n* was investigated by polarized optical microscopy (POM), differential scanning calorimetry (DSC), and X-ray diffraction (XRD) measurement. In the DSC thermograms, both ZI-11 and ZI-17 showed exothermic peaks, which is indicative of a phase transition from an isotropic liquid state to a mesomorphic state. Both ZI-11 and ZI-17 showed no birefringence under POM observation, which is characteristic of isotropic states (Figure 3-2 (a)). In order to verify the mesomorphic phases, ZI-*n* were investigated by XRD measurement. These studies revealed that ZI-17 formed well-ordered nanoarchitectures whereas ZI-11 did not. Our XRD system could not detect intense peaks in the range from $2\theta = 0°$ to 30° for ZI-11. On the other hand, ZI-17 showed intense peaks at 35.3, 30.5, 23.3, 21.7, 19.3, 18.5, and 17.7 Å, which correspond to (211), (220), (321), (420), (400), (332), and (422) reflections of a bicontinuous cubic (Cub_{bi}) phase with *Ia*3*d* symmetry (Figure 3-2 (b)). The phase behavior of ZI-*n* is summarized in Figure 3-3.

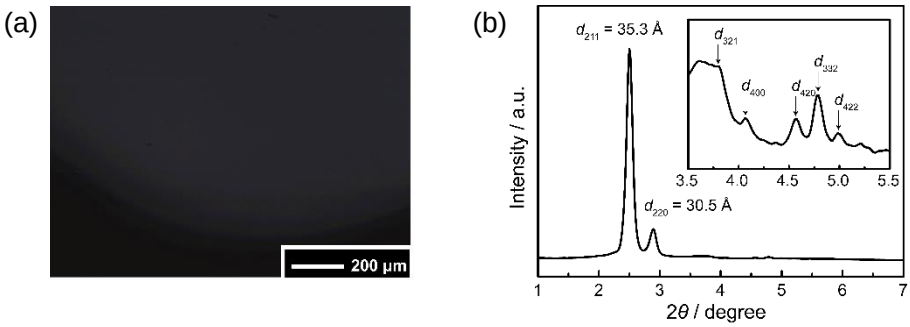

Figure 3-2. (a) POM image of ZI-17 in the Cub_{bi} phase at 150 °C. (b) XRD profile of ZI-17 in the Cub_{bi} phase at 140 °C.

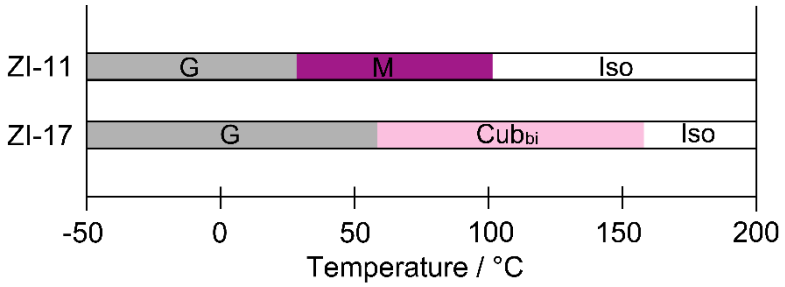

Figure 3-3. Thermotropic LC behavior of ZI-*n* on cooling. G, glassy; M, unidentified; Cub_{bi}, bicontinuous cubic; Iso, isotropic.

In chapter 2, the author determined that the phase behavior of the monomeric pyridinium-based amphiphilic zwitterions could be tuned by the addition of acids or salts. In this context, the author expected that that addition of acids or salts could tune the phase behavior of the gemini amphiphilic zwitterions. According to this idea, the author prepared the mixture of ZI-*n* and acids in order to exam the effect of acid addition on the phase behavior of gemini amphiphilic zwitterions. Bis(trifluoromethanesulfonyl)imide (HTf_2N) was chosen as an additive because the addition of HTf_2N is useful for changing the assembled structures of monomeric amphiphilic zwitterions due to its bulky structure. The mixtures of ZI-*n*/HTf_2N were prepared by slow evaporation of a methanol solution of ZI-*n* with an equimolar amount of HTf_2N per sulfonyl group. ZI-11/HTf_2N mixture was obtained as a homogeneous liquid at room temperature due to the lowering of the glass transition temperature (T_g) through the formation of ionic liquid-like ion pairs of imidazolium cation of ZI-11 and Tf_2N anion. The mesophase patterns of ZI-17 changed upon the addition of HTf_2N. ZI-17/HTf_2N mixture showed focal conic textures under POM observation, which is indicative of columnar (Col) phases (Figure 3-4 (a)). XRD measurement was also performed to investigate their assembled structures (Figure 3-4 (b)). ZI-17/HTf_2N mixture in a 1:2 molar ratio showed intense peaks at 34.2, 19.9, and 17.2 Å, which correspond to (100), (110), and (200) reflections of a hexagonal Col phase. The phase behavior of these samples is summarized in Figure 3-5.

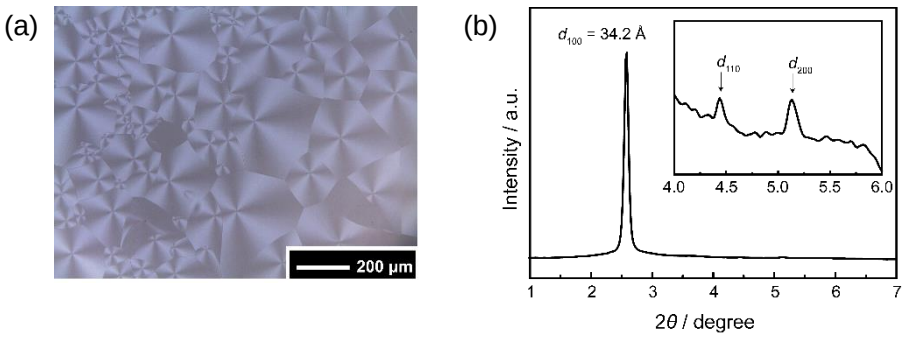

Figure 3-4. (a) POM image of ZI-17/HTf_2N in the Col phase at 65 °C. (b) XRD profile of ZI-17/HTf_2N mixture in the Col phase at 50 °C.

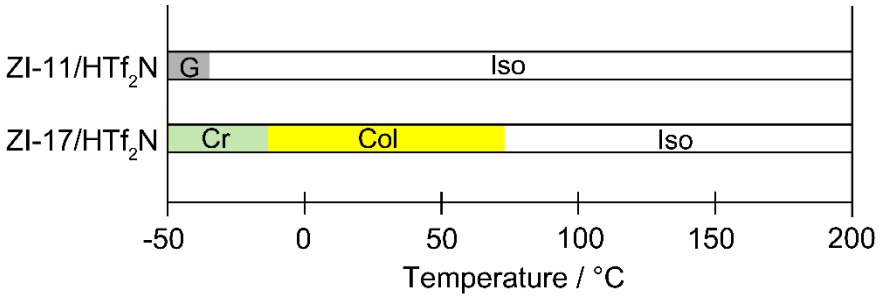

Figure 3-5. Thermotropic LC behavior of ZI-*n*/HTf_2N mixtures on cooling. G, glassy; Cr, crystalline; Col, columnar; Iso, isotropic.

To analyze the effect of HTf_2N addition to ZI-17 on their assembling properties, the author prepared ZI-17/HTf_2N mixtures in various ratios (Figure 3-6). The mesophase patterns changed from the Cub_{bi} phase to the Col phase with an increase of the molar ratio of HTf_2N in the mixtures. ZI-17/HTf_2N mixtures in 4:1, 2:1, and 4:3 molar ratios showed no birefringence under POM observation, suggesting the presence of the Cub_{bi} phases, while ZI-17/HTf_2N mixture in 1:1 and 1:2 molar ratios formed the Col phases. These results suggest that the addition of HTf_2N led to the expansion of the volume fraction of the ionophilic parts of ZI-17, which led to the mesophase pattern changes. These results suggest that combining amphiphilic zwitterions and acids or salts is useful to control nanoarchitectures of not only monomeric amphiphilic zwitterions but also gemini amphiphilic zwitterions.

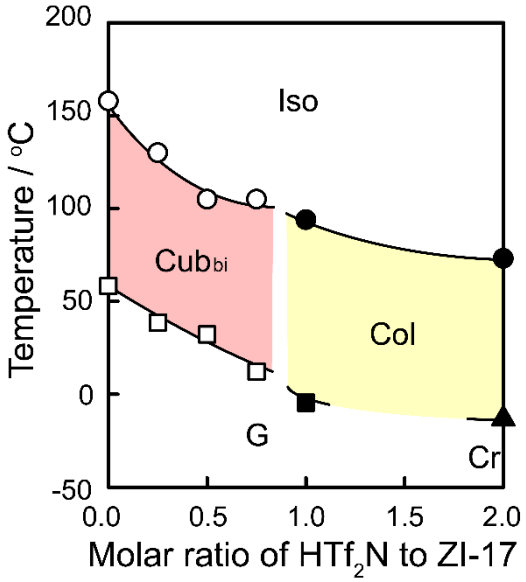

Figure 3-6. Phase diagram of ZI-17/HTf_2N mixtures. G, glassy; Cr, crystalline; Cub_{bi}, bicontinuous cubic; Col, columnar; Iso, isotropic.

3-2-3 Ion Conduction Properties of Gemini Amphiphilic Zwitterions

Ion conduction measurement also suggested that gemini amphiphilic zwitterions self-organized into well-ordered nanoarchitectures. ZI-17/HTf_2N mixture in a 2:1 molar ratio that formed the Cub_{bi} phase and ZI-17/HTf_2N mixture in a 1:2 molar ratio that formed the Col phase were chosen to study the ion conduction behavior. Nanosegregated LC assemblies were previously shown to have efficient ion conduction behavior dependent on their morphology when forming a monodomain (note that most nanosegregated LC assemblies form polydomains). To understand the characteristics of the Col structure formed by ZI-17/HTf_2N mixture in a 1:2 molar ratio, the author prepared two samples, each with a different macroscopically homogeneous alignment (either perpendicular or parallel to the electric field). The fabrication of a monodomain was achieved by mechanical shearing according to the literature.[11] Figure 3-7 shows ion conduction behavior of the present materials. Anisotropic ion conduction behavior was clearly observed for these samples. The ionic conductivity of ZI-17/HTf_2N mixture in a 1:2 molar ratio with parallel alignment in the Col phase increased with elevating temperatures and slightly decreased upon the phase transition from the Col to isotropic liquid state. The ionic conductivity of the mixture with perpendicular alignment increased in the measurement temperature ranges. The author also examined ion conduction behavior of ZI-17/HTf_2N mixture in a 2:1 molar ratio that formed the Cub_{bi} phase. Although the ionic conductivity of ZI-17/HTf_2N mixture in a 2:1 molar ratio was lower than that of ZI-17/HTf_2N mixture in a 1:2 molar ratio, it showed structure-dependent ion conduction behavior without any alignment methods. The ionic conductivity of ZI-17/HTf_2N mixture in a 2:1 molar ratio increased with elevating temperature ranging from around 50 to 150 °C, while it rapidly decreased upon the phase transition from the Cub_{bi} to isotropic state. This ion conduction behavior is similar to that observed for ionic liquid crystals forming Cub_{bi} phases.

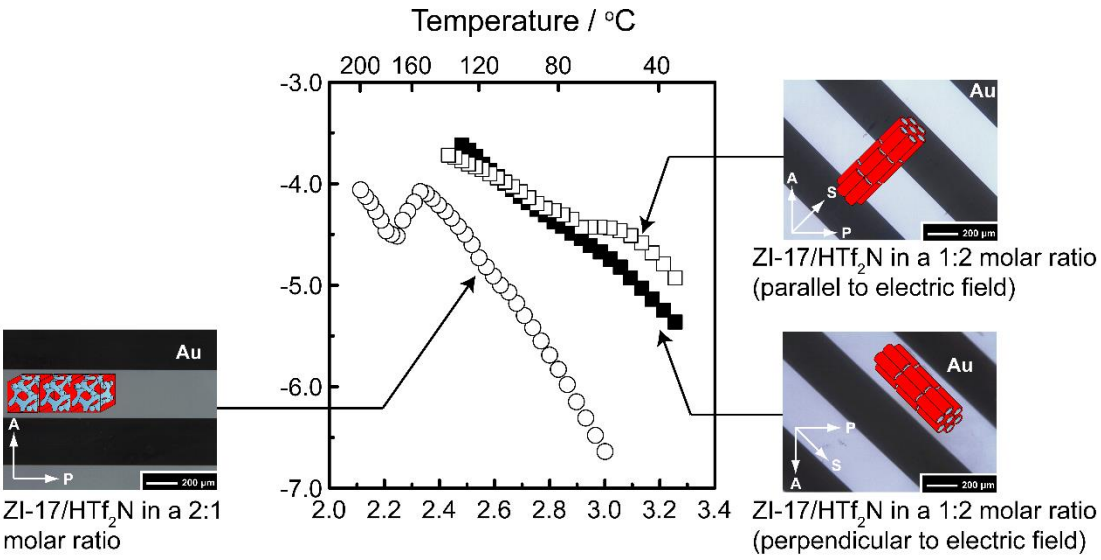

Figure 3-7. Ionic conductivities of ZI-17/HTf_2N mixture in a 1:2 molar ratio forming Col phase with parallel (□) and perpendicular (■) to the electric field and ZI-17/HTf_2N mixture in a 2:1 molar ratio forming Cub_{bi} phase (○). The POM image of them are also depicted.

3-3 Conclusion

A series of gemini zwitterions were synthesized and their phase behavior was investigated. The author successfully introduced thermotropic LC properties into gemini zwitterions by connecting gemini imidazolium-based zwitterions with long alkyl chains. The LC properties of ZI-17 changed upon the addition of HTf_2N by forming ionic liquid-like ion pairs between the imidazolium cation and Tf_2N anion. The exhibition of nanosegregated assemblies was also confirmed by ion conduction measurement. The mixture of ZI-17 and HTf_2N showed ion conduction properties derived from their assembled structures. These results suggest that gemini zwitterions have the potential to be employed as building blocks of thermotropic LC materials.

3-4 Experimental

General Procedures

^1H NMR spectra was obtained on a JEOL NMR spectrometer (α-500). Chemical shifts of ^1H signals were quoted to $(CH_3)_4Si$ (δ = 0.00) as an internal standard. Elemental analysis was carried out on an Elementar Analytical vario EL3. Thermal properties of the materials were examined with a DSC using DSC-6220, Seiko Instruments. Heating and cooling rate was 5 °C min^{-1}. A polarizing optical microscope, Olympus BX51 equipped with a Lincam hot-stage, was used for observation of LC phases.

XRD patterns were obtained using a Rigaku RINT-2500 diffractometer with CuKα radiation. The ionic conductivity was measured with an impedance analyzer Solartron 1260 (Schlumberger). The heating rate was 2 °C min^{-1}.

Materials

All chemical reagents and solvents were obtained from commercial sources and used without purification. All reactions were carried out in anhydrous solvents under an argon atmosphere.

Synthesis

A series of ZI-*n* were synthesized according to the literature.[7a] The synthetic pathway was depicted in Scheme 3-1. Followed by deprotonation of 2-alkylimidazole, the crude was treated with 1,6-dibromohexane to yield Im-*n*. Subsequent quaternization reaction of I*m*-n with 1,3-propanesultone gave ZI-*n*.

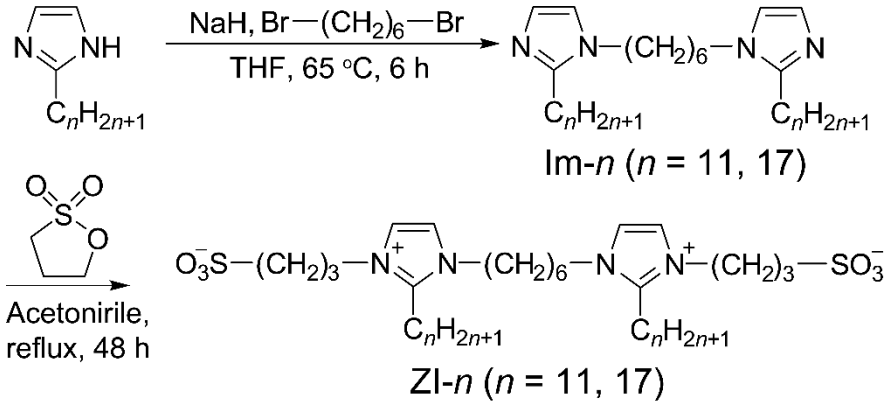

Scheme 3-1. Synthesis of gemini imidazolium-based amphiphilic zwitterions (ZI-*n*) used in this study.

Im-17

Anhydrous THF (250 ml) was charged into 500 ml flask and sodium hydride (60 wt%, dispersion in paraffin liquid, 3.34 g, 83.5 mmol) was added. 2-heptadecylimidazole (22.22 g, 72.5 mmol) was added slowly and the mixture was stirred at room temperature. After several minutes, the mixture was warmed at 40 °C for an hour. Followed by these procedures, 1,6-dibromohexane (7.26 g, 29.8 mmol) was added slowly and stirred at 65 °C for 6 hours. Then water was added slowly in order to stop the reaction, and the obtained aqueous solution was concentrated by rotary evaporation. Then water and chloroform were added, and the organic layer was separated and washed with water. The resulting organic phase was dried over anhydrous $MgSO_4$ and concentrated by rotary evaporation. The crude product was purified by flash column chromatography (silica gel, eluent: chloroform/MeOH = 10/1).

The crude product was recrystallized from acetone to give Im-17 as a white solid.
^{1}H NMR (500 MHz, $CDCl_3$): δ = 6.94 (d, *J* = 1.5 Hz, 2H), 6.78 (d, *J* = 1.0 Hz, 2H), 3.81 (t, *J* = 7.5 Hz, 4H), 2.61 (d, *J* = 8.0 Hz 4H), 1.78-1.70 (m, 8H), 1.40-1.21 (m, 60H), 0.88 (t, *J* = 6.75 Hz, 6H).

ZI-17

1,3-propanesultone (3.17 g, 26.0 mmol) was added to a solution of Im-17 (3.01 g, 4.32 mmol) in acetonitrile (40 ml) and refluxed for 48 h. The crude product was recrystallized from isopropanol to give ZI-17 (3.00 g; 3.19 mmol; 73.8 %) as a white solid.
^{1}H NMR (500 MHz, $CDCl_3$): δ = 7.87 (d, *J* = 2.5 Hz, 2H), 7.72 (d, *J* = 1.5 Hz, 2H), 4.41 (t, *J* = 6.5 Hz, 4H), 4.16 (d, *J* = 7.25 Hz, 4H), 3.07 (t, *J* = 7.5 Hz, 4H), 2.75 (t, *J* = 6.5 Hz, 4H), 2.37 (m, 4H), 1.92 (m, 8H), 1.58-1.25 (m, 60 H), 0.88 (t, *J* = 7.0 Hz, 6H). Elemental analysis. Calcd for $C_{52}H_{98}N_4O_6S_2$ 1.0H_2O: C, 65.23; H, 10.53; N, 5.85. Found: C, 64.96; H, 10.14; N, 5.94.

ZI-11

^{1}H NMR (500 MHz, $CDCl_3$): δ = 7.87 (m, 2H), 7.73 (m, 2H), 4.41 (t, *J* = 6.25 Hz, 4H), 4.16 (d, *J* = 7.0 Hz, 4H), 3.07 (t, *J* = 7.75 Hz, 4H), 2.76 (t, *J* = 7.00 Hz, 4H), 2.35-2.31 (m, 8H), 1.94 (m, 4H), 1.58-1.25 (m, 36 H), 0.88 (t, *J* = 7.0 Hz, 6H). Elemental analysis. Calcd for $C_{40}H_{74}N_4O_6S_2$ 1.5H_2O: C, 60.19; H, 9.72; N, 7.02. Found: C, 60.31; H, 9.47; N, 6.72.

3-5 References

1. M. Henmi, K. Nakatsuji, T. Ichikawa, H. Tomioka, T. Sakamoto, M. Yoshio, T. Kato, *Adv. Mater*., **2012**, *24*, 2238.
2. Y. Ishida, Y. Kai, S. Kato, A. Misawa, S. Amano, Y. Matsuoka, K. Saigo, *Angew. Chem. Int. Ed.*, **2008**, *47*, 8241.
3. (a) K. Binnemans, *Chem. Rev*., **2005**, *105*, 4148. (b) T. Kato, T. Yasuda, Y. Kamikawa, M. Yoshio, *Chem. Commun*., **2009**, 729.
4. T. Kato, N. Mizoshita, K. Kishimoto, *Angew. Chem., Int. Ed.*, **2006**, *45*, 38.
5. F. M. Menger, J. S. Keiper, *Angew. Chem. Int. Ed.*, **2000**, *39*, 1907.
6. M. In, R. Zana, *J. Dispersion Sci. Technol*., **2007**, *28*, 143.
7. (a) J. E. Bara, E. S. Hatakeyama, B. R. Wiesenauer, X. Zeng, R. D. Noble, D. L. Gin, *Liq. Cryst.*, **2010**, *37*, 1587. (b) T. Zhou, J. Zhao, *J. Colloid Interface Sci.*, **2009**, *338*, 156. (c) Y. Wang, E. F. Marques, *J. Phys. Chem. B*, **2006**, *110*, 1151. (d) M. Yang, K. Stappert, A.-V. Mudring, *J. Mater. Chem. C*, **2014**, *2*, 458.
8. J. L. Anderson, R. Ding, A. Ellern, D. W. Armstrong, *J. Am. Chem. Soc*., **2005**, *127*, 593.

9. (a) S. Fuller, N. N. Shinde, G. J. T. Tiddy, G. S. Attard, O. Howell, *Langmuir*, **1996**, *12*, 1117. (b) M. Dreja, *Chem. Commun*. **1998**, *13*, 1371.
10. P. Wasserscheid, T. Welton, Eds. *Ionic Liquids in Synthesis*, 2nd ed.; Wiley-VCH: Weinheim, Germany, **2007**.
11. M. Yoshio, T. Mukai, H. Ohno, T. Kato, *J. Am. Chem. Soc*., **2004**, *126*, 994.

Chapter 4

Microphase-Separated Assemblies through the Block Copolymerization of Zwitterions

Chapter 4

4-1 Introduction

Poly(ionic liquid)s, in which either cations or anions of ionic liquids are covalently bound to the polymer chain, are rapidly emerging as neoteric polyelectrolytes to traditional ones.[1] They show low glass transition temperatures (T_g) in spite of their high charge density. In the last decades, a number of poly(ionic liquid)s have been designed and synthesized to apply them into various applications.[2] In particular, considerable efforts have been devoted to develop their electrolyte performance.[3] The representative strategy is block copolymerization of poly(ionic liquid)s.[4] Block copolymers are one of the self-organizing soft materials forming microphase-separated assemblies. Thus, this approach is expected to yield a new subclass of polyelectrolytes having high ionic conductivity, due to the low T_g of ionic liquids, and also good mechanical stability deriving from the other component. Another strategy is zwitterionization of poly(ionic liquid)s.[5] We have previously reported that some polyzwitterions are capable of forming a homogeneous complex with some lithium salts. The obtained mixtures function as polyelectrolytes transporting ions of additives. According to these studies, the author envisioned that a marriage between the two strategies, block copolymerization and zwitterionization, would be one of the potential approaches to expand the potential applications of ionic liquid-based materials for various fields, such as electrolyte researches. In this chapter, the author designed and synthesized polyzwitterion block copolymers and examined their material properties.

4-2 Results and Discussion

4-2-1 Molecular Design

Our block copolymers, PS-*b*-PZI-*x* (the index *x* is the mol% of the polyzwitterion unit in a block copolymer) were synthesized by the following procedure (Scheme 4-1). Polystyrene-*b*-poly(2-(dimethylamino)ethyl acrylate) (PS-*b*-PDMA-*x*) was synthesized by reversible addition-fragmentation chain transfer polymerization, according to the literature.[6] Three types of PS-*b*-PDMA-*x* were prepared: PS-*b*-PDMA-19.7 (M_n: 16.4 kg/mol), PS-*b*-PDMA-44.1 (M_n: 6.64 kg/mol), and PS-*b*-PDMA-64.3 (M_n: 10.8 kg/mol). PS-*b*-PDMA-19.7 was synthesized by elongation of the DMA monomer from polystyrene (PS) (M_n = 12.4 kg/mol) and the others were synthesized from PS (M_n = 3.39 kg/mol). The number average molecular weight was determined by ^{1}H NMR measurement and M_n for the initial PS determined by size exclusion chromatography (SEC). A subsequent quaternization reaction of the amine groups of these three types of PS-*b*-PDMA-*x* with 1, 3-propanesultone gave polystyrene-*b*-poly(2-(dimethyl-(3-sulfopropyl)-ammonium betaine)ethyl acrylate) (PS-*b*-PZI-*x*) block copolymers. By comparing the ^{1}H NMR spectra of PS-*b*-PDMA-64.3 and PS-*b*-PZI-64.3, the author found that

the quaternization reaction of the amine groups into zwitterion groups proceeded quantitatively. The molecular characteristics for PS-*b*-PZI-*x* were not examined because this family was slightly soluble in conventional solvents. This is because the molecule contains two segments with opposite polarities.

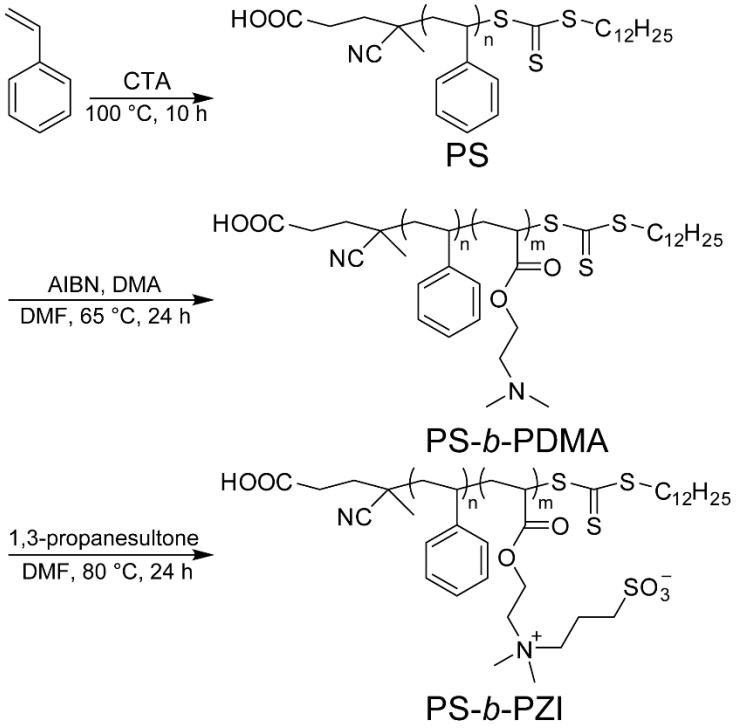

CTA: 4-cyano-4-[(dodecylsulfanylthiocarbonyl)sulfanyl]pentanoic acid
DMA: 2-(dimethylamino)ethyl acrylate

Scheme 4-1. Synthesis of PS-*b*-PZI

4-2-2 Self-Organization Behavior of Polyzwitterion Block Copolymers

PS-*b*-PZI-64.3 showed dispersion behavior in H_2O upon looking at its solubility in conventional solvents. The author performed ^1H NMR measurement of PS-*b*-PZI-64.3 in D_2O to examine the dispersion mechanism (Figure 4-1). No signals corresponding to the PS block were observed, indicating that PS-*b*-PZI-64.3 formed micelles with a PS core and PZI shell in D_2O. Block copolymers are known to form core-shell micelles in selective solvents for one of their blocks. Comparing the dispersion behaviour of PS-*b*-PZI-64.3 with that of the other PS-*b*-PZI-*x*, the dispersion of PS-*b*-PZI-*x* was found to decrease with the decrease of the PZI composition.

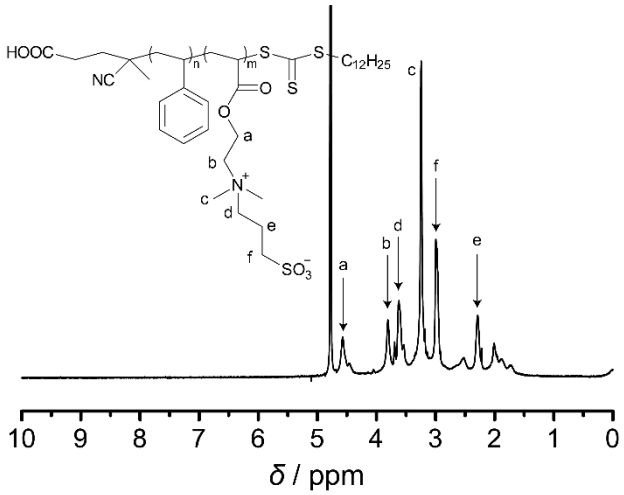

Figure 4-1. ^{1}H NMR spectrum of PS-*b*-PZI-64.3 in D_2O.

If the condensation of the dispersed PS-*b*-PZI-*x* solutions in co-existence with lithium salts proceeds by forming and retaining ion pairs between the PZI segments and lithium salts, then the author expect a microphase-separated matrix to be formed in which PS cores form dispersed globular domains surrounded by a continuous ionic liquid-like domain composed of the PZI segments and lithium salts. Considering the dispersion behavior of a series of PS-*b*-PZI-*x* in H_2O, the author determined that PS-*b*-PZI-64.3 was the most suitable for preparing homogeneous microphase-separated assemblies among the obtained block copolymers. The author accordingly prepared a solution of PS-*b*-PZI-64.3 with an equimolar amount of lithium bis(trifluoromethanesulfonyl)imide ($LiTf_2N$) per zwitterion unit in H_2O (7 % w/w), and cast it onto a substrate using a pipette. Slow evaporation of the solvent at 70 °C, followed by vacuum drying for 4 hours at 70 °C resulted in the formation of a film-state sample (PS-*b*-PZI-64.3/$LiTf_2N$ film). For comparison, pristine PS-*b*-PZI-64.3 film was also prepared according to similar procedures. The morphology of this film was investigated by transmission electron microscopy (TEM) and by small angle X-ray scattering (SAXS) measurements. In the SAXS patterns of both films, a single broad peak was observed at small angles, suggesting the formation of randomly aggregated micelles (Figure 4-2).

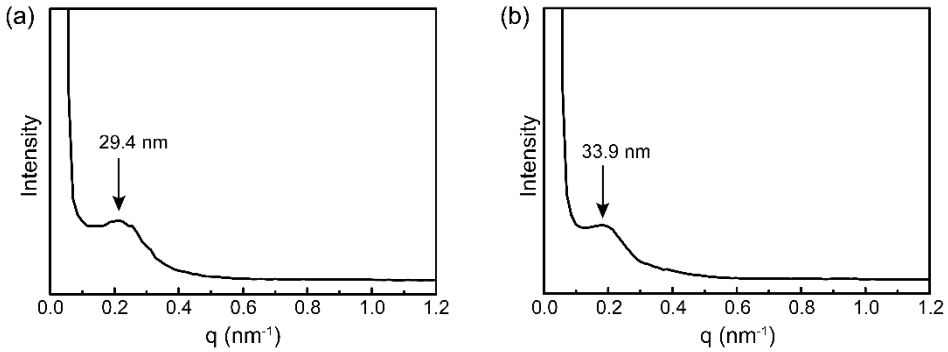

Figure 4-2. SAXS profiles of (a) PS-*b*-PZI-64.3 film and (b) PS-*b*-PZI-64.3/$LiTf_2N$ film.

TEM results provided further evidence that the micelle structures were maintained beyond the condensation process. TEM measurements were performed for the PS-*b*-PZI-64.3/$LiTf_2N$ film after the PS domains had been stained with OsO_4, and the film was sliced into sections using a glass knife (approximate thickness = 70 nm). Figure 4-3 shows a TEM image for the PS-*b*-PZI-64.3/$LiTf_2N$ film. The PS segments formed globular domains with a diameter of about 9 nm in the film. The number of PS-*b*-PZI-64.3 polymer chains forming a core-shell micelle was estimated to be about 80 assuming that the radius and density of the PS globular domains are 4.5 nm and 1.05 g/cm^3, respectively.

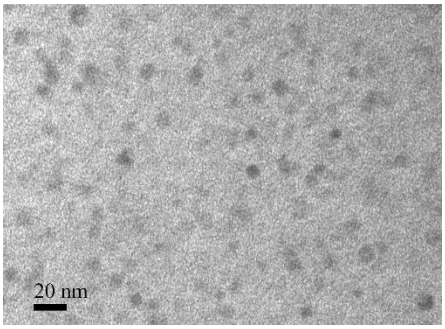

Figure 4-3. TEM image of PS-*b*-PZI-64.3/$LiTf_2N$ film. PS domains were darkened by OsO_4 staining.

To determine whether the PZI segments that form a complex with $LiTf_2N$ set up ionic liquid-like domains around the PS core domains in the condensed state, the author performed DSC measurement on the film. Upon heating, a glass transition behavior was observed at 122 °C for PS-*b*-PZI-64.3, whereas T_g = 78 °C for the PS-*b*-PZI-64.3/$LiTf_2N$ film. The author attributes this decrease in T_g to the formation of ionic liquid-like ion pairs between the ammonium cation of the PZI segments and the Tf_2N anion of the added $LiTf_2N$, through the

hard and soft acids and bases principle. To gain further insight, the author prepared a PZI-homopolymer and examined its thermal behavior in the presence and absence of $LiTf_2N$. As well as PS-*b*-PZI, PZI-homopolymer underwent a decrease of T_g upon the addition of $LiTf_2N$, from 150 °C to 83 °C, which was approximately the same as the T_g for PS-*b*-PZI-64.3/$LiTf_2N$ film. From these comparisons, the author concludes that the condensation of the polyzwitterion block copolymer and lithium salts causes the formation of a microphase-separated matrix consisting of PS cores and ionic liquid-like shell domains.

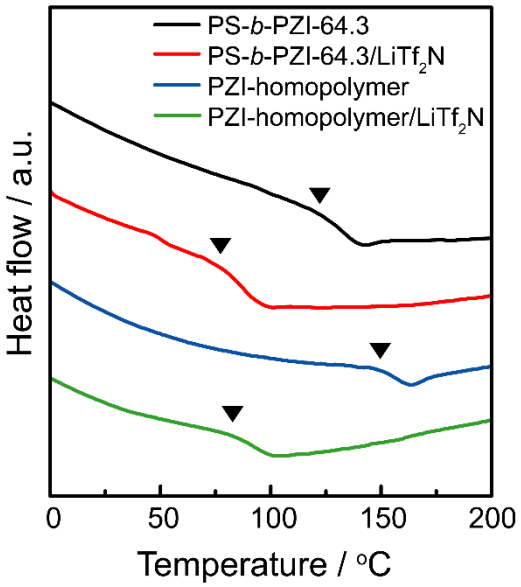

Figure 4-4. DSC thermograms of obtained samples on heating. Filled markers denote T_g.

4-2-3 Ion Conduction Behavior of Polyzwitterion Block Copolymers

The ionic conductivities of the resulting films were measured over a range of temperatures. Figure 4-5 shows Arrhenius plots of the conductivities as a function of temperature. The ionic conductivity of PS-*b*-PZI-64.3 film was very low, and was below the detection limit of our system at temperatures below about 150 °C. In contrast, ion conduction behavior was observed very clearly for PS-*b*-PZI-64.3/$LiTf_2N$ film. For example, the ionic conductivity of PS-*b*-PZI-64.3 film was 1.2×10^{-10} S cm^{-1} at 150 °C, and that of PS-*b*-PZI-64.3/$LiTf_2N$ film was 3.8×10^{-7} S cm^{-1} at 146 °C. These results support our conclusion that the PZI segments preferentially interact with $LiTf_2N$ and set up an ionic liquid-like environment in the microphase-separated assembly. For comparison, the author also measured the ionic conductivity of PZI-homopolymer/$LiTf_2N$ film. Although the ionic conductivity of PS-*b*-PZI-64.3/$LiTf_2N$ film was

slightly lower than that of PZI-homopolymer/$LiTf_2N$ film, the activation energies of these two films were similar over a broad range of temperatures. For example, the activation energies of the PS-*b*-PZI-64.3/$LiTf_2N$ film and the PZI-homopolymer/$LiTf_2N$ at temperatures between 80 °C and 120 °C were calculated to be 184 and 173 kJ mol^{-1}, respectively. These results suggest that the PS core domains are located in the film without preventing the PZI/$LiTf_2N$ shell domains from forming a macroscopically continuous ion conductive pathway.

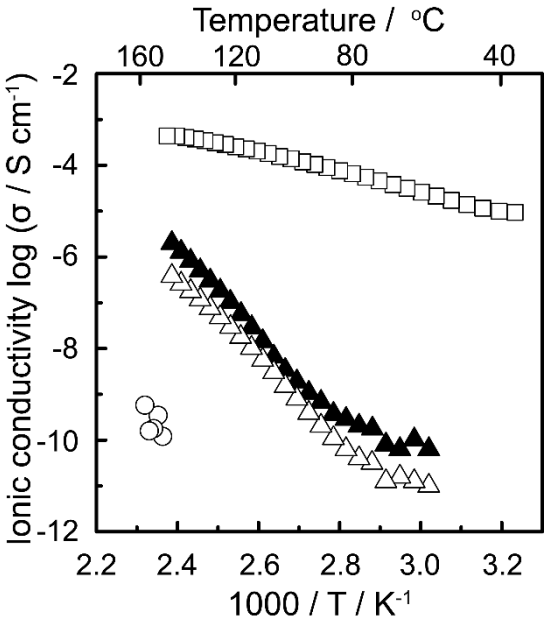

Figure 4-5. Ionic conductivities of PS-*b*-PZI-64.3 film (○), PS-*b*-PZI-64.3/$LiTf_2N$ film (△), PZI-homopolymer/$LiTf_2N$ film (▲) and PS-*b*-PZI-64.3/phosphoric acid film (□) on heating.

Recently, zwitterions have been studied for the development of proton conductive materials because of their ability to dissociate acids.[7] The author expected that a combination of PS-*b*-PZI-64.3 and acids would lead to the construction of a microstructured matrix for proton conduction. Phosphoric acid was selected because it possesses thermal stability over a wide range of temperatures. The author prepared PS-*b*-PZI-64.3/phosphoric acid film by a similar procedure and studied its ion conduction behavior. The ionic conductivity of PS-*b*-PZI-64.3/phosphoric acid film was 9.9×10^{-6} S cm^{-1} at 40 °C, which increased linearly as elevating temperature until 150 °C with the activation energy of 40 kJ mol^{-1}, indicating that the PZI segments enhanced the proton dissociation of phosphoric acid. Compared to PS-*b*-PZI-64.3/$LiTf_2N$ film, the PS-*b*-PZI-64.3/phosphoric acid film had a greater ionic conductivity and

lower activation energy. These differences can be explained by assuming that ion conductive property of PS-*b*-PZI-64.3/$LiTf_2N$ film is dominated by vehicle mechanism while that of PS-*b*-PZI-64.3/phosphoric acid film is based both on vehicle and hopping (Grotthuss) mechanism[8] via hydrogen bonding network of bound water molecules which remain around PZI segments even after vacuum drying and heating processes. Zwitterionic compounds are known to bind water molecules strongly via electrostatically induced hydration.[9]

4-3 Conclusion

In conclusion, the author has demonstrated that the aggregation of core-shell micelles formed by a poly(styrene-*b*-ammonium-based zwitterion) block copolymer resulted in the formation of microphase-separated ion active polymer films. By preparing films in the co-existence with a lithium salt, the resulting polymer films acquire ion conductive properties, which is due to the ability of polyzwitterion segments to form an ionic liquid-like environment with lithium salts. Furthermore, the ionic conductivities of the polyzwitterion block copolymer and polyzwitterion homopolymer in the presence of lithium salts were similar in the measurement temperature range. These results suggest that the material design demonstrated here would be an effective way to introduce new properties onto polyzwitterions without losing their intrinsic properties.

4-4 Experimental

General procedures

^1H NMR was obtained on a JNM-ECX400 and JNM-ECA500 (JEOL). Chemical shifts of ^1H signals were quoted to tetramethylsilane or 3-(trimethylsilyl)-1-propanesulfonic acid sodium salt (δ = 0.00) as internal standard. Elemental analysis was carried out on an Elementar Analytical vario EL3. Polydispersity were determined by SEC systems composed on degassing unit DGU-20A, durable pump LC-20AD, column oven CTO-20AC, UV-vis detector SPD-20A, refractive index detector RID-20A (Shimadzu), and column Asaphipak GF-7M HQ (shodex). SEC measurement was performed at 40 °C using DMF containing 10 mM LiBr or THF as an eluent at a flow rate of 0.4 ml/min. A calibration curve was prepared using polystyrene standard. Small angle X-ray scattering (SAXS) profiles were obtained using a Smart Lab (Rigaku) with CuKα radiation. Samples for transmission electron microscopy (TEM) were exposed to the vapor of 4 wt% of aqueous OsO_4 for 20 min and sectioned using an FC7 cryomicrotome (Leica) at -120 °C using a glass knife at 70 nm thickness. Sections were placed on Cu grids. TEM micrographs were obtained by JEM-2100 (JEOL) operating at 200 kV. The thermal properties were examined by DSC-6220 (Seiko Instruments). The heating and

cooling rates were 10 °C min^{-1}. The ionic conductivity was measured with an impedance analyzer Solartron 1260 (Schlumberger). The heating rate was 2 °C min^{-1}.

Materials

All chemical reagents and solvents were obtained from commercial sources. Both styrene and 2-(dimethylamino)ethyl acrylate were distilled before use. AIBN was purified via recrystallization. The other reagents were used without purification. All reactions were carried out in anhydrous solvents under an argon atmosphere.

Synthesis

PS

Styrene (52.8 g, 0.507 mol) and 4-cyano-4-[(dodecylsulfanylthiocarbonyl)sulfanyl] pentanoic acid (0.526 g, 1.30 mmol) were charged into a 200 mL Schlenk flask and subjected to three freeze-pump-thaw cycles. After stirring at 100 °C for 10 h, it was placed into liquid nitrogen. The product was purified by reprecipitation procedures with methanol and vacuum dried. Yield: 7.36 g of yellow powder. SEC (DMF containing 10 mM LiBr, 40 °C): M_n = 3.39 kg/mol, M_w/M_n = 1.57 (against PS standards). The SEC trace and ^{1}H NMR spectrum were depicted in Figure 4-6 and 4-7, respectively.

PS-*b*-PDMA-64.3

PS (1.00 g, 0.294 mmol), 2-(dimethylamino)ethyl acrylate (8.02 g, 56.0 mmol), AIBN (3.37 mg, 0.0205 mmol) and DMF (10 ml) were charged into a 30 ml Schlenk flask and subjected to three freeze-pump-thaw cycles. After stirring at 65 °C for 24 h, it was placed into liquid nitrogen. The product was purified by reprecipitation procedures with hexane and vacuum dried. Yield: 2.34 g of yellow oil. M_n and M_w/M_n determined by the combination of ^{1}H NMR and SEC measurement: M_n = 10.8 kg/mol, M_w/M_n = 1.96. Elemental analysis. Calcd: C, 67.9; H, 8.74; N, 6.84. Found: C, 67.7; H, 8.96: N, 6.53. The SEC trace and ^{1}H NMR spectrum were depicted in Figure 4-6 and 4-7, respectively.

PS-*b*-PZI-64.3

1, 3-propane sultone (4.45 g, 0.0364 mol), PS-*b*-PDMA-64.3 (0.663 g, 0.0614 mmol) and DMF (40 mL) were charged into a 100 ml Schlenk flask, which was stirred at 80 °C for 24 h. The product was purified by reprecipitation procedures with methanol and vacuum dried. Yield: 0.657 g of yellow powder. Elemental analysis. Calcd for PS-*b*-PZI H_2O per ZI unit: C, 51.0; H, 7.55; N, 4.09. Found: C, 49.5; H, 7.54: N, 3.93.

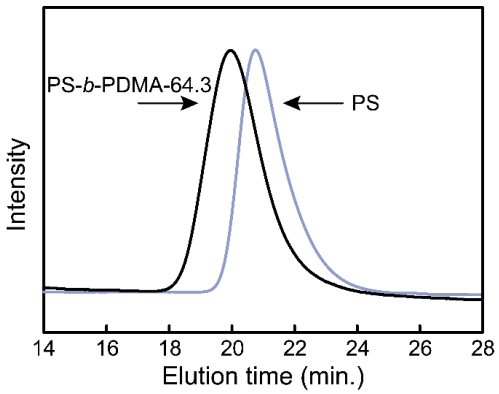

Figure 4-6. SEC traces of PS and PS-*b*-PDMA-64.3.

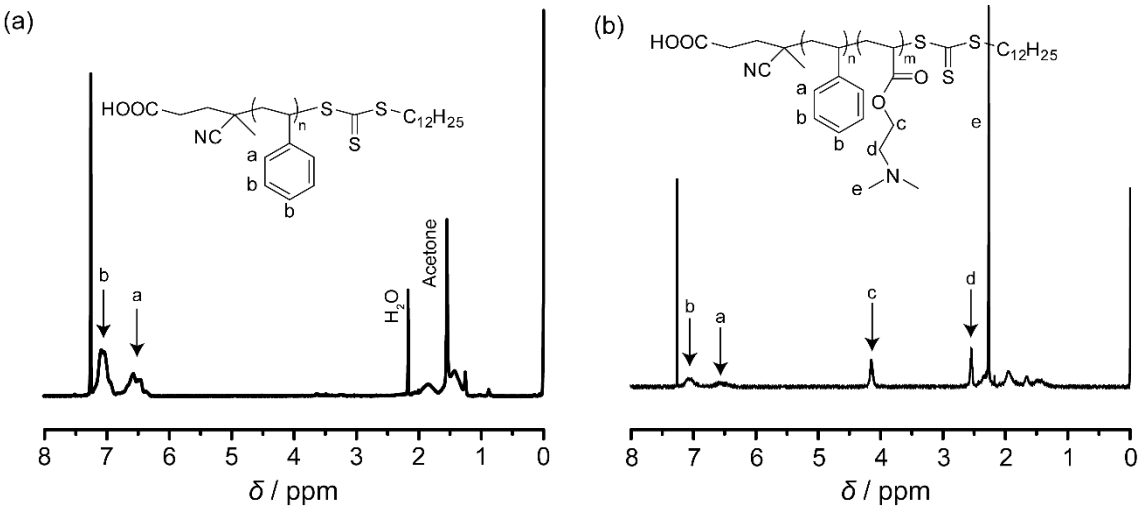

Figure 4-7. ^{1}H NMR spectra of (a) PS and (b) PS-*b*-PDMA-64.3 in $CDCl_3$.

4-5 References

1. (a) H. Ohno, K. Ito, *Chem. Lett.*, **1998**, *27*, 751. (b) N. Nishimura, H. Ohno, *Polymer*, **2014**, *55*, 3289.
2. (a) J. Lu, F. Yan, J. Texter, *Prog. Polym. Sci.*, **2009**, *34*, 431. (b) D. Mecerreyes, *Prog. Polym. Sci.*, **2011**, *36*, 1629.
3. (a) E. B. Anderson, T. E. Long, *Polymer*, **2010**, *51*, 2447. (b) J. Yuan, M. Antonietti, *Polymer*,

2011, *52*, 1469. (d) J. Yuan, D. Mecerreyes, M. Antonietti, *Prog. Polym. Sci*., **2013**, *38*, 1009.

4. (a) Y. Gu, T. P. Lodge, *Macromolecules*, **2011**, *44*, 1732. (b) R. L. Weber, Y. Ye, A. L. Schmitt, S. M. Banik, Y. A. Elabd, M. K. Mahanthappa, *Macromolecules*, **2011**, *44*, 5727. (c) M. D. Green, D. Wang, S. T. Hemp, J.-H. Choi, K. I. Winey, J. R. Heflin, T. E. Long, *Polymer*, **2012**, *53*, 3677. (d) V. F. Scalfani, E. F. Wiesenauer, J. R. Ekblad, J. P. Edwards, D. L. Gin, T. S. Bailey, *Macromolecules*, **2012**, *45*, 4262. (e) Y. Ye, S. Sharick, E. M. Davis, K. I. Winey, Y. A. Elabd, *ACS Macro Lett*., **2013**, *2*, 575.
5. M. Yoshizawa, M. Hirao, K. I. Akita, H. Ohno, *J. Mater. Chem*., **2001**, *11*, 1057.
6. (a) G. Moad, E. Rizzardo, S. H. Thang, *Aust. J. Chem*., **2005**, *58*, 379. (b) G. Moad, E. Rizzardo, S. H. Thang, *Aust. J. Chem*., **2009**, *62*, 1402. (c) J.-H. Choi, Y. Ye, Y. A. Elabd, K. I. Winey, *Macromolecules*, **2013**, *46*, 5290.
7. (a) M. Yoshizawa, H. Ohno, *Chem. Commun*., **2004**, 1828. (b) B. Soberats, M. Yoshio, T. Ichikawa, S. Taguchi, H. Ohno, T. Kato, *J. Am. Chem. Soc*., **2013**, *135*, 15286.
8. K.-D. Kreuer, *Chem. Mater*., **1996**, *8*, 610.
9. (a) Z. Cao, Q. Yu, H. Xue, G. Cheng, S. Jiang, *Angew. Chem. Int. Ed*., **2010**, *49*, 3771. (b) T. Ichikawa, T. Kato, H. Ohno, *J. Am. Chem. Soc*., **2012**, *134*, 11354.

Chapter 5

Conclusions

Chapter 5

Conclusions

In this thesis, the author introduced self-organizing properties into zwitterions to expand the designability of ionic liquid-based materials. The author employed zwitterions and polyzwitterions as building blocks of liquid-crystalline materials and block copolymers respectively, and their assembled states and properties were discussed.

Chapter 1 introduced the self-organizing ionic liquids and zwitterions. The objective of this thesis was also described.

In chapter 2, a series of pyridinium-based amphiphilic zwitterions were prepared. While pristine zwitterions exhibited only smectic liquid-crystalline phase, the addition of lithium salts or acids induced nanosegregated phases, such as bicontinuous cubic phase and smectic phase, depending on the additive anion species. The mesophase pattern changes were attributed to the formation of ionic liquid-like ion pairs composed of the cation of zwitterions and the anion of salts or acids added, which was confirmed with Raman spectroscopic measurement. Moreover, the amphiphilic zwitterions were found to show both thermotropic liquid-crystalline behavior and lyotropic liquid-crystalline behavior in the presence of polar solvents, such as protic ionic liquids. These results indicate that the combination of amphiphilic zwitterions and suitable additive ions is a potential method to construct nanostructured liquid-crystalline materials with tunable phase behavior. Ion conduction measurement also revealed that the obtained bicontinuous cubic assemblies formed 3D continuously connected ion active surface.

In chapter 3, the author focused on the use of zwitterions as the ionophilic part of gemini amphiphiles to expand the design of self-organizing zwitterions. A series of gemini imidazolium-based amphiphilic zwitterions were designed and synthesized. Through the comparison of self-organization behavior of gemini amphiphilic zwitterions in the presence and absence of an acid, it was revealed an imidazolium salt exhibited the bicontinuous cubic phase and its mesophase pattern changed from the bicontinuous cubic to columnar phase upon the addition of an acid. Ion conduction measurement also revealed that the obtained liquid-crystalline materials showed morphology dependent ion conduction behavior.

In chapter 4, poly(zwitterion-*b*-styrene) block copolymers were prepared to induce the exhibition of microphase-separated structures of polyzwitterions. They have the ability to form micelles composed of a polystyrene core and polyzwitterion shell in water. Aggregation of these micelles in the presence of lithium salts or acids provides polymer films with micellar aggregates. Ion conduction

measurement revealed that 3D continuous polyzwitterion shell domains transported cations of the additives. Through the comparison of ion conduction behavior between poly(zwitterion-*b*-styrene) block copolymers and polyzwitterion homopolymer in the presence of lithium salts, it was shown that the polystyrene cores dispersed in the block copolymer film without losing the intrinsic polyzwitterion properties.

Throughout this thesis, the author provided two strategies for the introduction of self-organizing properties into zwitterions. One was the use of nanosegregated assemblies through the introduction of liquid-crystalline properties into zwitterions. The other was the use of microphase-separated assemblies through the block copolymerization of polyzwitterions. The author concluded that the introduction of self-assembly ability to zwitterions is an effective way to induce new properties onto zwitterions. Namely, the formation of nanosegregated assemblies using zwitterions led to unique ion conductive properties derived from nanoarchitectures, which enables efficient proton transportation. The formation of microphase-separated assemblies has the potential to add incompatible functions into polyzwitterions while maintaining their intrinsic ion conduction properties. The author believes that combining the features of zwitterions and self-organizing materials would lead to the expansion of the designability for the development of functional ionic liquid-based materials.

Chapter 5

List of Publications

Original papers

(1) “Design of Amphiphilic Zwitterions Forming Liquid-Crystalline Phases and Effects of Lithium Salts Addition on Their Phase Behavior”
Takuro Matsumoto, Takahiro Ichikawa, Junji Sakuda, Takashi Kato, and Hiroyuki Ohno
Bull. Chem. Soc Jpn., **2014**, *87*, 792.

(2) “Design of ionic liquid-based polyelectrolytes by combining ‘nanostructurisation’ and ‘zwitterionisation’”
Takuro Matsumoto, Takahiro Ichikawa, and Hiroyuki Ohno
Polym. Chem., **2016**, *7*, 1230.

(3) “Thermotropic liquid-crystalline properties of gemini imidazolium-based amphiphilic zwitterions”
Takuro Matsumoto, Takahiro Ichikawa, Takashi Kato, and Hiroyuki Ohno
In preparation.

(4) “Gelation of an amino acid ionic liquid by the addition of a phosphonium-type zwitterion”
Satomi Taguchi, Takuro Matsumoto, Takahiro Ichikawa, Takashi Kato, and Hiroyuki Ohno
Chem. Commun., **2011**, *47*, 11342.

(5) “Liquid-Crystalline Electrolytes for Lithium-Ion Batteries: Ordered Assemblies of a mesogen-Containing Carbonate and a Lithium Salt”
Junji Sakuda, Eiji Hosono, Masafumi Yoshio, Takahiro Ichikawa, Takuro Matsumoto, Hiroyuki Ohno, Haoshen Zhou, and Takashi Kato
Adv. Funct. Mat., **2015**, *25*, 1206.

Books

(1) 松本拓郎、黒田浩介、税田祥平、鶴巻晃子、阿部充、田口怜美、藤田恭子、西村直美、中村暢文、大野弘幸、「イオン液体の略称」イオン液体サーキュラー　第 1 号、2013

Chapter 5

Acknowledgements

This work was performed between April 2010 and March 2016 at Tokyo University of Agriculture and Technology under the supervision of Professor Hiroyuki Ohno.

First, the author would like to express deepest gratitude to Professor Hiroyuki Ohno. He gave the author continuous support and encouragement. Without his help, the author would not be fascinated with researches and this thesis would not be accomplished. The author learned many valuable life-lessons from him.

The author would like to express his great appreciation to Professor Nobuhumi Nakamura for his continuous encouragement and support. He gave the author many valuable suggestion for his research and life.

The author would like to express his great appreciation to Associate Professor Takahiro Ichikawa. He taught the author how to perform and enjoy research. Owing to his helpful advices, the author could finish his doctoral thesis.

The author is deeply grateful to Professor Takashi Kato at the University of Tokyo for warm collaboration on the structure analysis for liquid-crystalline compounds. He gave the author helpful suggestion and supports.

The author is deeply grateful to Dr. Satomi Taguchi. She taught the author the basics of experiment and presentation.

The author would like to acknowledge Dr. Kyoko Fujita, Dr. Naomi Nishimura, Dr. Yuki Kohno, Dr. Miyuki Masuda, Dr. Mitsuru Abe, Dr. Shohei Hayakawa, Dr. Akiko Tsurumaki, Dr. Kosuke Kuroda, Dr. Shohei Saita, and Dr. Kouta Takeda. They provided the author with helpful advices.

The author would like to acknowledge Ms. Yoko Kayama, Ms. Kanae Fujimura, Mr. Akiyoshi Okafuji, Mr. Gantsetseg Ankhbayar, Mr. Hiroaki Takeuchi, and Ms. Saki Fujiwara for their grateful support.

The author also would like to thank to Dr. Junji Sakuda at the University of Tokyo for collaborating on X-ray diffraction measurement for his samples.

The author also expresses his appreciation to all members of the Ohno-Nakamura laboratory.

The author is grateful for financial support from the JSPS Research Fellowship for Young Scientist from April 2015 to March 2016.

Finally, the author expresses his deep gratitude to his mother Sadako Matsumoto for her continuous support and encouragement.

February 2016

Takuro Matsumoto